DP-1409

603149

REACTIVITY AND REACTION RATE MEASUREMENTS IN U-D_2O LATTICES WITH COAXIAL FUEL

D. J. PELLARIN AND B. M. MORRIS

SAVANNAH RIVER LABORATORY
AIKEN, SOUTH CAROLINA 29801

PREPARED FOR THE U.S. ENERGY RESEARCH AND DEVELOPMENT ADMINISTRATION UNDER CONTRACT AT(07-2)-1

NOTICE

Printed in the United States of America

Available from
National Technical Information Service
U.S. Department of Commerce
5285 Port Royal Road
Springfield, Virginia 22161

Price: Printed Copy $5.00; Microfiche $3.00

DP-1409
Distribution Category: UC-34c

REACTIVITY AND REACTION RATE MEASUREMENTS IN U-D_2O LATTICES WITH COAXIAL FUEL

by

D. J. Pellarin and B. M. Morris

Approved by

P. L. Roggenkamp, Research Manager
Reactor Physics Division

Publication Date: December 1976

E. I. DU PONT DE NEMOURS AND COMPANY
SAVANNAH RIVER LABORATORY
AIKEN, SOUTH CAROLINA 29801

PREPARED FOR THE U. S. ENERGY RESEARCH AND DEVELOPMENT ADMINISTRATION UNDER CONTRACT AT(07-2)-1

ABSTRACT

Integral reaction rate parameters, intracell thermal neutron flux profiles, and material bucklings were measured for D_2O-moderated uniform lattices in the exponential facility at the Savannah River Laboratory. Two different slightly enriched coaxial uranium fuel assemblies were examined over a wide range of triangular lattice pitches. Integral parameters are reported for inner and outer fuel separately providing data for a more detailed and rigorous comparison with computation than has been previously available. Results are compared with RAHAB calculations using ENDF/B-IV cross sections. Large discrepancies in agreement between calculation and experiment, outside of experimental errors and uncertainties in the input cross sections, probably result from the resonance capture models used by RAHAB.

CONTENTS

LIST OF TABLES

LIST OF FIGURES

REACTIVITY AND REACTION RATE MEASUREMENTS IN U-D_2O LATTICES WITH COAXIAL FUEL

INTRODUCTION

In recent years, a high degree of sophistication in representing the physics of thermal reactors has been achieved through the development of detailed transport theory codes such as HAMMER and RAHAB.[1,2] These codes are used extensively at the Savannah River Laboratory (SRL) for reactor physics lattice calculations in design and safety studies.

A fundamental goal of the calculational program at SRL is to provide accurate representation of reactivity and reaction rate ratios over a wide range of D_2O-thermal reactor lattices (including mixed lattices and enriched uranium lattices). This effort involves the improvement of theoretical and model formalisms as well as the use of the latest ENDF/B cross sections.

A broad base of experimental evidence is required to assess the performance of the theoretical methods and differential cross sections used for predicting integral reactor properties such as reactivity or reaction rates. The most meaningful evaluations occur for clean lattices with simple geometry and composition so that errors of representation in the theoretical methods are minimized. Two H_2O-moderated lattices of slightly enriched uranium rods[3,4] and three D_2O-moderated lattices of natural uranium rods[3,5] traditionally have been used as benchmarks for these evaluations.

The purpose of this work is to expand the experimental data base to include uniform lattices of coaxial fuel assemblies. The neutron moderation within the fuel coolant annuli and the mutual resonance shielding afforded by the concentric fuel tubes are effects that do not occur in simple rod lattices. To emphasize these effects, integral parameters for the inner and outer fuel have been presented separately. The coaxial fuel lattice experiments thus provide diagnostic data for a more detailed and rigorous comparison with computation than has been available previously.

SUMMARY

Reactivity and reaction rate parameters were measured for D_2O-moderated uniform lattices in the exponential facility (SE-SP)[6,7] at SRL. Two different slightly enriched, coaxial, uranium fuel assemblies were examined over a wide range of triangular lattice pitches. The lattice experiments with Type I fuel (Table 1) were performed at 5.5-, 6.0-, 7.0-, and 8.0-inch triangular pitches with D_2O purities of 99.50 to 99.35 mol %. The lattice experiments with Type II fuel were performed at 6.36-, 7.0-, 8.08-, 9.25-, and 14.0-inch triangular pitches with D_2O purities of 99.54 to 99.13 mol %.

Parameters that were derived from experimental data are summarized as follows:

^{238}U (n,γ) Capture Ratio	ρ_{28}	$= \frac{\text{Epicadmium } ^{238}U \text{ Captures}}{\text{Subcadmium } ^{238}U \text{ Captures}}$
^{235}U Fission Capture Ratio	δ_{25}	$= \frac{\text{Epicadmium } ^{235}U \text{ Fissions}}{\text{Subcadmium } ^{235}U \text{ Fissions}}$
^{238}U Fast Fissions	δ_{28}	$= \frac{^{238}U \text{ Fissions}}{^{235}U \text{ Fissions}}$
Modified Conversion Ratio	C^*	$= \frac{^{238}U \text{ Captures}}{^{235}U \text{ Fissions}}$
Thermal Neutron Spectral Index	R	$= \frac{[^{176}Lu/^{63}Cu]^{\text{Subcadmium}}_{\text{Fuel}}}{[^{176}Lu/^{63}Cu]^{\text{Subcadmium}}_{\text{Thermal Reference}}}$
Material Buckling	B_m^2	= Radial Buckling (B_R^2) + Axial Buckling (B_Z^2)

Intracell thermal neutron activation and spectral index profiles also were measured.

The measurements were compared with RAHAB[2] calculations using ENDF/B-IV cross sections with the following results:

- Calculated material bucklings are consistently lower than measurement for both fuel types. The discrepancies correspond to errors in k_{eff} of from 4 to 8% with the largest disagreement at the lower pitches.

- Calculated values of ρ_{28} for both fuel types are higher than measurement. ρ_{28} for the outer fuel is overpredicted by about 20%, the Type I inner fuel by about 4%, and the Type II inner fuel by about 11%.

- RAHAB overpredicts δ_{25} for both fuel types by about 23% for the inner fuel and about 14% for the outer fuel.

- RAHAB generally overpredicts C^* for both fuel types by about 8% for the inner fuel and about 4% for the Type II outer fuel.

- RAHAB underestimates δ_{28} for both fuel types by about 11% for the inner fuel and about 7% for the outer fuel.

- RAHAB properly predicts the qualitative behavior of spectrum hardening but overestimates the magnitude of the effect both in the fuel and in the moderator. Calculated values of R exceed the measured values by about 4% in the Type II fuel and by about 2% in the Type I fuel.

- The agreement between calculated and measured intracell thermal neutron activation profiles is good.

The overprediction of ρ_{28}, C^*, and δ_{25} and the underprediction of δ_{28} are consistent with the underprediction of the material buckling and keff by RAHAB.[3] The magnitudes of the discrepancies are larger than uncertainties in input cross sections, experimental uncertainties, or possible systematic bias in the experimental methods. The most probable source of discrepancy is the theoretical treatment of resonance capture in the RAHAB calculations.

EXPERIMENTAL DETAILS

Experimental Facilities

Material bucklings and reaction rate parameters were measured in the exponential facility (SE-SP)[6,7] at SRL.

The SP is an enriched-uranium fueled, graphite-moderated, H_2O-cooled reactor. The core consists of a graphite-filled cylinder inside a 5-ft graphite cube. A 4-ft graphite cube on one side of the SP forms a thermal column used to irradiate reference foils in a purely thermal flux simultaneously with the reaction rate experiments in the SE.

The SE, a 3/8-inch-thick aluminum cylinder, 5 ft in diameter and 7 ft high, is mounted directly over the SP. The sides of the tank are covered with 1/8 inch of cadmium. The tank is supported from above by structural steel beams. Grid beams at the top of the SE, a bottom positioning plate, and top spacers were used to support and accurately space the fuel assemblies at each of the lattice pitches. A cylindrical graphite pedestal is mounted between the SE tank and the SP reactor to minimize spatial harmonics in the SE. A cadmium shutter (1/8-inch-thick) can be inserted between the pedestal and the SE tank to permit the measurement of the distribution of fast leakage neutrons that enter the SE tank through the graphite pedestal and from scatter off the walls in the reactor room. This distribution can be used to correct the flux shapes measured in the SE without the shutter in place. The SP-SE facility is shown in Figure 1. Storage tanks and a closed piping system supply D_2O moderator to the SE tank.

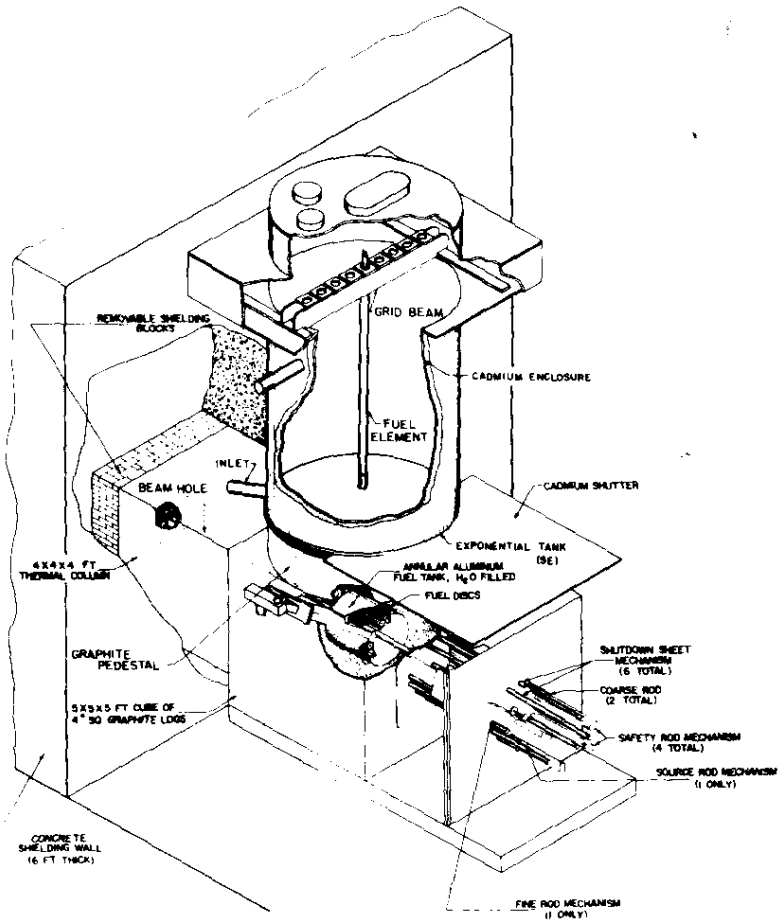

FIGURE 1. SP-SE Facility

Equilibrium flux spectra, characteristic of the measured lattices, existed in the central region of the SE where the experimental data were obtained. This was affirmed by radial and axial cadmium ratio mapping measurements using gold pin detectors. In each case, a region of constant cadmium ratio was noted.

Description of Fuel Assemblies

The Type I and Type II fuel assemblies consisted of nested inner and outer fuel pairs stacked on an aluminum inner housing to produce uniform, continuous, coaxial fuel columns. In Table 1, the two fuel assembly types are shown in cross section, and the geometries and compositions are summarized. The assemblies differ in ^{235}U content, in size, and in the volume ratio of fuel to contained D_2O. This ratio is ~2 for the Type I fuel and ~1 for the Type II fuel.

TABLE 1

Assembly Geometry and Fuel Composition

	Type I	*Type II*
Al Inner Housing, inches		
Outer Diameter[a]	0.8706	1.6512
Inner Diameter	0.5320	1.4730
Inner Fuel Slug, inches		
Al Cladding[b]		
Outer Diameter[a]	1.9975	2.6787
Inner Diameter	1.166	1.958
Fuel		
Outer Diameter[a]	1.914	2.605
Inner Diameter	1.226	2.018
Outer Fuel Slug, inches		
Al Cladding[b]		
Outer Diameter[a]	3.076	3.700
Inner Diameter	2.400	3.105
Fuel		
Outer Diameter[a]	3.016	3.640
Inner Diameter	2.460	3.165
Fuel Composition, wt %		
^{235}U	0.860	1.10
^{238}U	99.101	98.877
^{236}U	0.032	0.023

a. Includes rib volumes.
b. A thin (0.5 mil for Type I fuel; 0.41 mil for Type II inner fuel; 0.47 mil for Type II outer fuel) nickel flashing at the fuel-cladding interface was homogenized in the cladding for the calculations.

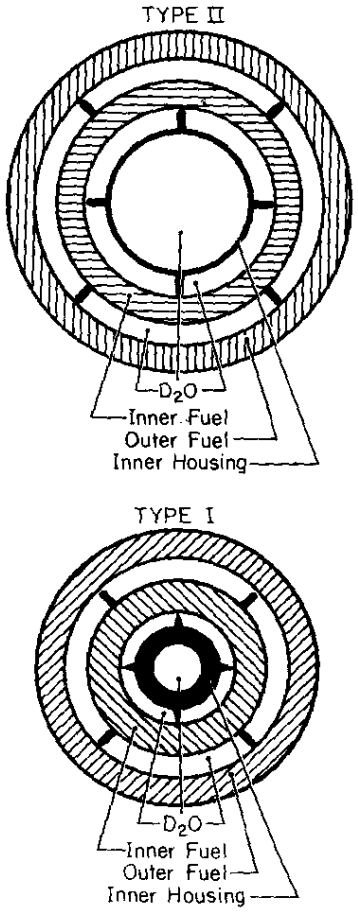

Description of Lattices

The SE lattice arrangements corresponding to each of the activation experiments with the Type I fuel are shown in Figure 2. Various numbers of enriched fuel spikes (~100 g/ft of ^{235}U) were included in the low reactivity 5.5- and 6.0-inch pitch lattices to increase the flux level at the foil irradiation assembly located at the center of the SE. Errors in the reaction rate measurements do not occur from the use of spikes at the periphery of the lattice provided the neutron spectrum within the center lattice cell where the measurements are made is unaffected by the addition of the spikes. No appreciable spectrum distortion was anticipated based on a previous study of the spectrum effects of adding spikes for a similar lattice.[8] In all cases, the buckling experiments were performed without spikes in the lattices.

The SE lattice arrangements corresponding to each of the activation experiments with the Type II fuel are shown in Figure 3. The lattices for the buckling measurements were the same as the corresponding lattices for the activation except a standard Type II fuel assembly was used at the center position.

Description of Irradiation Assembly

The foil-bearing irradiation assembly was identical to the other lattice fuel assemblies except that an inner and outer fuel pair with accurately machined central angle slots to accommodate thin, bare, arc-shaped foils and thick filler pieces was located near the center of the fuel column. The Type II fuel irradiation pieces are shown in Figure 4. Although cladding was removed in the region of the slots during machining, replacement aluminum cladding pieces were fabricated and installed for the irradiations. The foil-bearing assembly was placed in the center of the SE lattice and rotated at 3 rpm on its axis during the irradiations to obtain an azimuthal average of the radial flux in the cell.

Foil Details

Arc-shaped foils were placed between the filler pieces used in the machined slots of the inner and outer irradiation fuel pair (Figure 4). The foils were made to fit accurately the central angle subtended by the slot so that the specific activation of the foil represented the average reaction rate in the fuel. Fission product contamination of the foils was prevented by interposing 0.001-inch-thick aluminum at uranium interfaces. Epicadmium activations were obtained from 0.272-inch-diameter foils placed inside small (0.375-inch-diameter × 0.100-inch-thick) cadmium pill boxes contained in a recess in the lower filler piece 2.5 inches from the nearest measurement position.

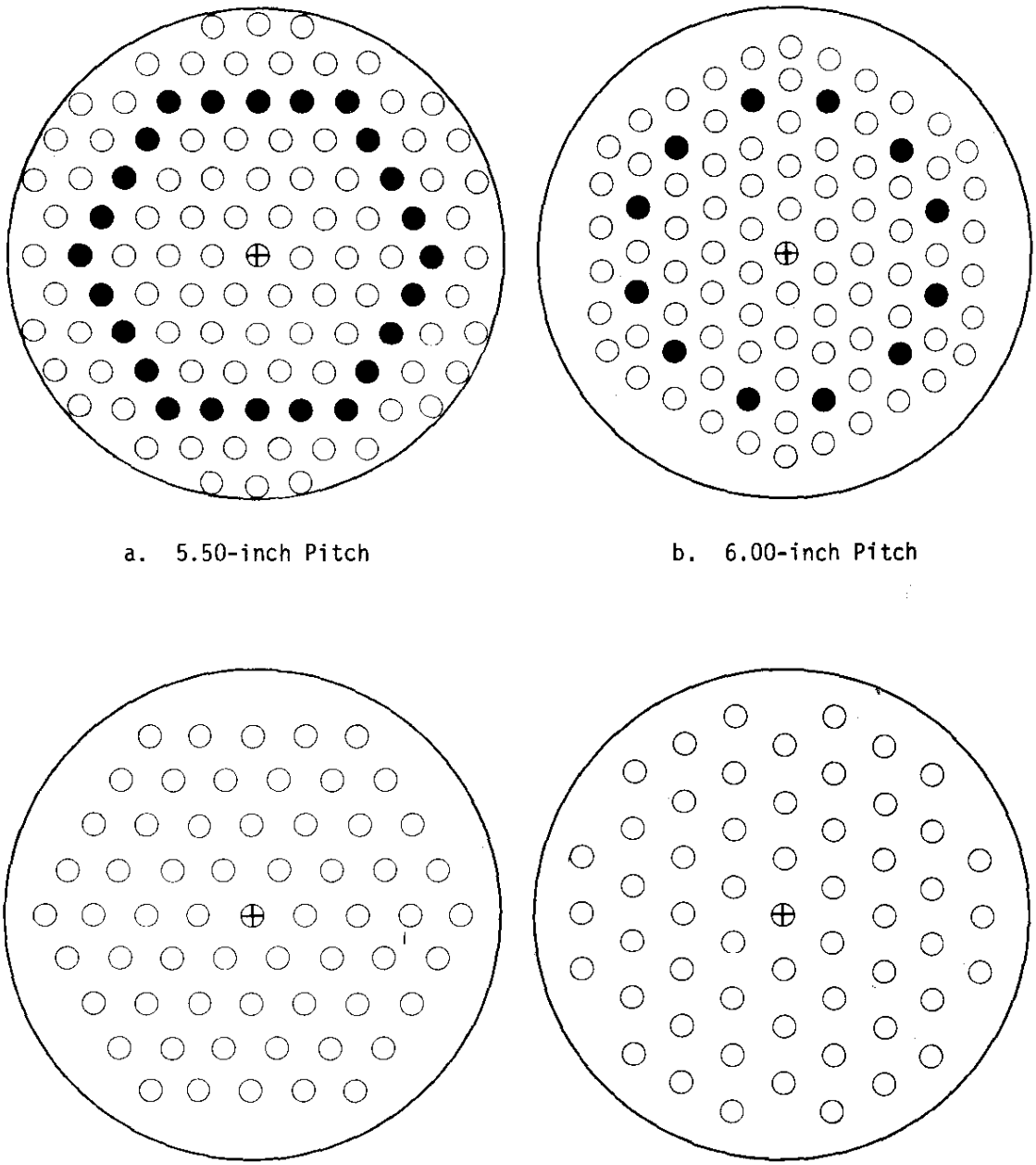

FIGURE 2. SE Lattice Arrangements for Experiments with Type I Fuel

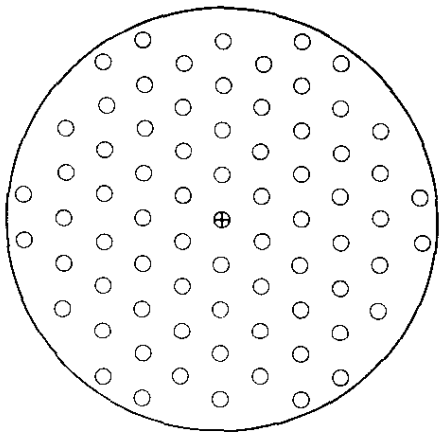

a. 6.35-inch Pitch

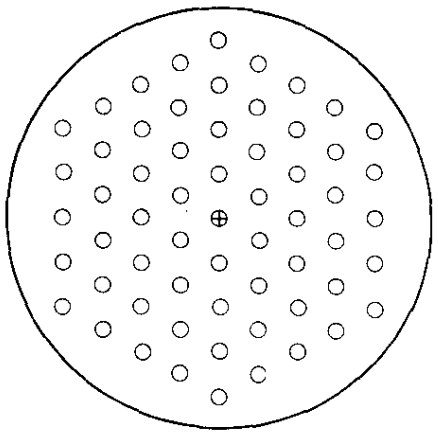

b. 7.00-inch Pitch

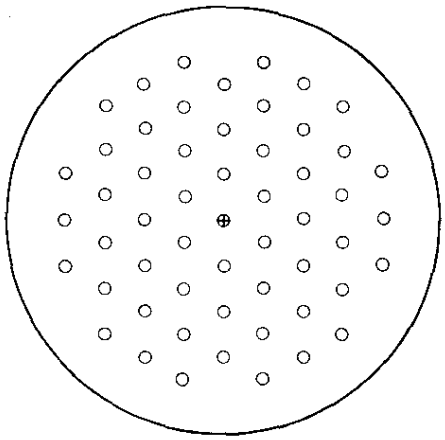

c. 8.08-inch Pitch

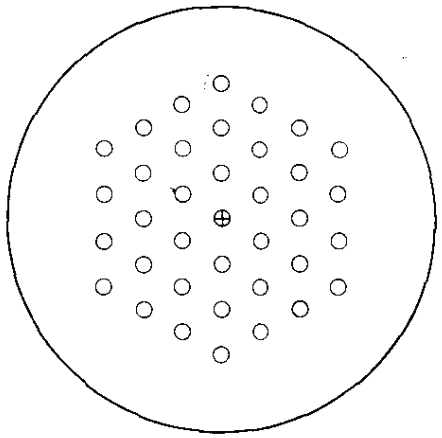

d. 9.25-inch Pitch

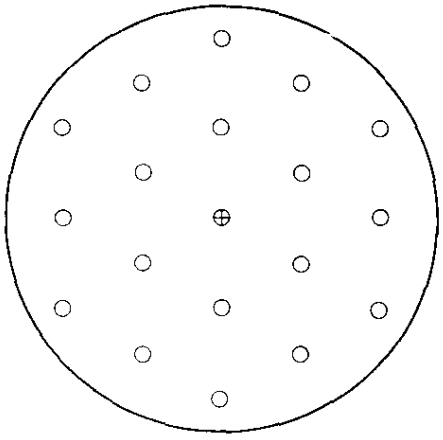

e. 14.00-inch Pitch

⊕ Foil Irradiation Fuel Assembly
○ Type II Fuel Assembly

FIGURE 3. SE Lattice Arrangements for Experiments with Type II Fuel

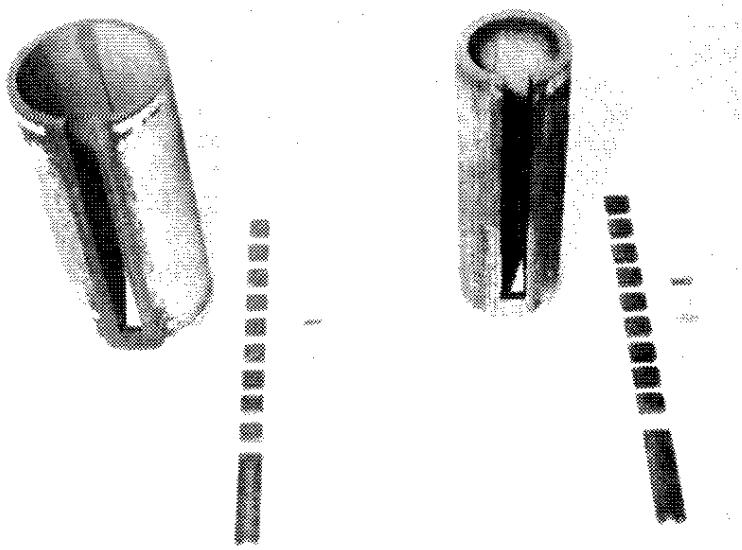

FIGURE 4. Inner and Outer Fuel Pieces for Foil Experiments with Type I Fuel

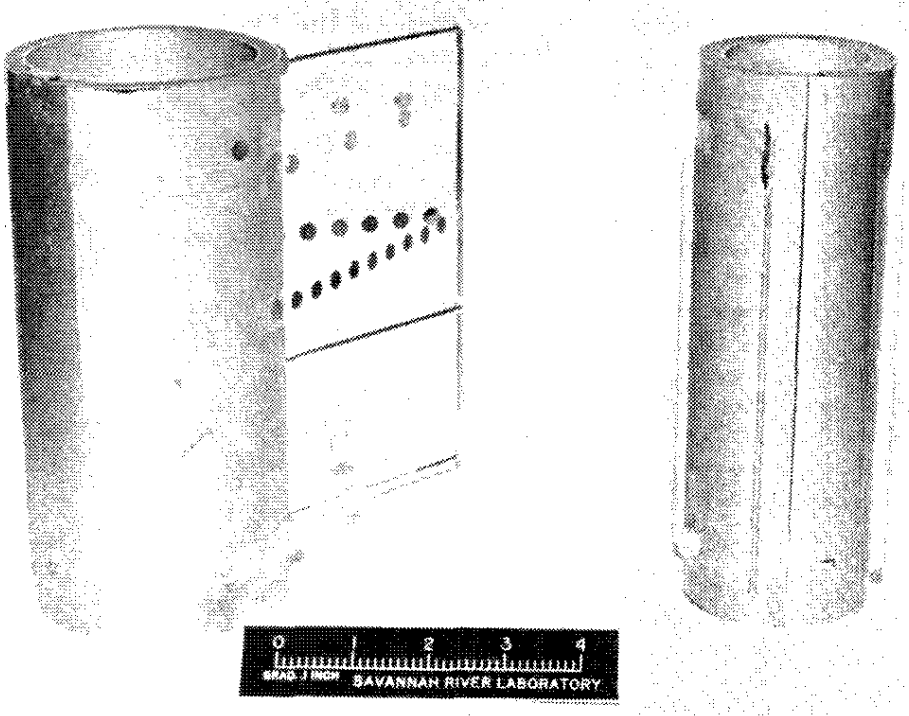

FIGURE 5. Inner and Outer Fuel Pieces Showing External Foil Loading for Type II Fuel

A well-thermalized position for activating reference foils in a thermal neutron flux was established 10 to 14 inches inside the 3-inch-diameter thermal column of the SP (Figure 1). The reference foils were mounted on two aluminum discs (A and B spinners, Table 3) that were rotated at 1 rpm during the exposure. Relative exposure histories for the reference foils in the thermal column and the sample foils in the SE lattice were identical because the SP supplied irradiation neutrons simultaneously to both. The measured cadmium ratio (0.032-inch cadmium) for thin (0.002-inch) gold at the thermal reference position is approximately 2800, which gives an equivalent 1/v cadmium ratio of 3×10^4. No corrections for epicadmium activation were required to the reference foil activities.

Bare and cadmium-covered 0.272-inch-diameter lutetium-copper-lutetium and copper foils were suspended in the moderator on 1/2-inch-wide strips of 1-mil polyester tape supported on a 3/32-inch-diameter aluminum wire frame (Figure 5). This frame was supported at the ends by small aluminum cylinders epoxied to the surface of the outer fuel cylinder. Templates were used to provide precise placement of the foils on the tape before affixing to the frame. The cell radius was calculated for each foil position based on geometrical considerations.

Table 2 shows a typical foil loading in the fuel with a summary of the foil materials, dimensions, and uses. A similar summary for the foils used in the thermal reference is given in Table 3.

A description of the foil materials used in the experiments and the gamma counting procedures are given in Table 4. The gamma activities of the foils were counted with sodium iodide (NaI) scintillation spectrometers. Corrections were made for the small differences in foil-to-counter geometry between the various shaped foils. Since small foil-to-counter acceptance angles were used, this correction generally was about 0.3%. The data output from the counting equipment was in the form of punched paper tape and teletype printout. The paper tapes were processed, and the data were corrected for deadtime, background, foil weight, gamma attenuation, and radioactive decay.

TABLE 2

Typical Foil Loading Arrangement in the Fuel

Foil Material	*Thickness, inch*	*Foil Size*	*Inner and Outer Fuel Representation*	*Use*
Cu	0.0105	Shaped	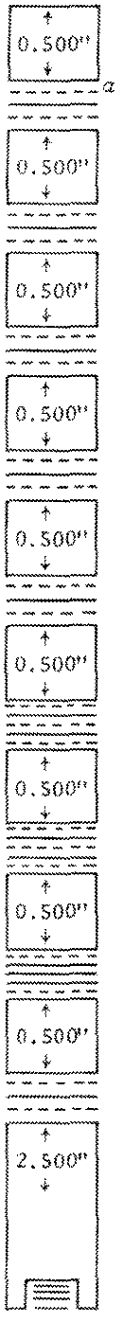 [a]	ρ_{28}, Thermal Flux Profile
Depl U	0.0032	Shaped		ρ_{28}, C*
Depl U	0.0032	Shaped		ρ_{28}, C*
Cu	0.0105	Shaped		ρ_{28}, Thermal Flux Profile
^{235}U-Al	0.0055	Shaped		δ_{25}
Nat U Depl U	0.0043 0.0032	Shaped		ρ_{28}, C*, δ_{28}
Nat U Depl U	0.0043 0.0032	Shaped		ρ_{28}, C*, δ_{28}
Lu Cu Lu	0.020 0.0105 0.020	Shaped		R
Cu	0.0105	Shaped		ρ_{28}, Thermal Flux Profile
Cadmium Pill Box				
Lu	0.020			
Cu	0.0105			R, ρ_{28}, Thermal Flux Profile
Cu	0.0105			
^{235}U-Al	0.0055	0.272" Dia		δ_{25}

a. 1-mil-thick Al foil is represented by dashed line (---)

TABLE 3

Typical Foil Loading Arrangement in the Thermal Reference

A Spinner

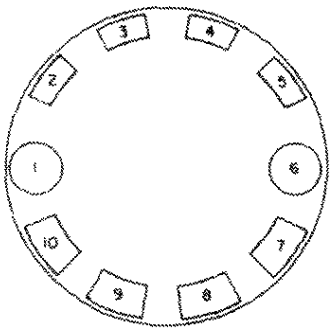

B Spinner

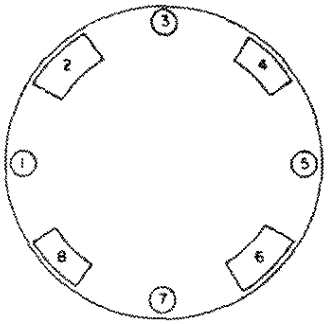

Foil Location	*Foil Material*	*Thickness, inch*	*Foil Size*	*Use*
A Spinner				
1	Depl	0.0032	0.500" Dia	ρ_{28}, C* Counter Geometry Correction
2	Depl	0.032	Shaped-Outer	ρ_{28}, C*, Counter Geometry Correction
3	Cu	0.0105	Shaped-Outer	ρ_{28}, C*
4	Cu	0.0105	Shaped-Outer	ρ_{28}, C*
5	Nat U	0.0043	Shaped-Outer	ρ_{28}, C*, Counter Geometry Correction
6	Nat U	0.0043	0.500" Dia	ρ_{28}, C* Counter Geometry Correction
7	Nat U	0.0043	Shaped-Inner	ρ_{28}, C*, Counter Geometry Correction
8	Cu	0.0105	Shaped-Inner	ρ_{28}, C*
9	Cu	0.0105	Shaped-Inner	ρ_{28}, C*
10	Depl	0.0032	Shaped-Inner	ρ_{28}, C*, Counter Geometry Correction
B Spinner				
1	Lu	0.020	0.272" Dia	Spectral Index Measurements
	Cu	0.0105	" "	
	Lu	0.020	" "	
2	Lu	0.020	Shaped-Inner	Spectral Index Measurements
	Cu	0.0105	" "	
	Lu	0.020	" "	
3	Lu	0.020	0.272" Dia	Spectral Index Measurements
	Cu	0.0105	" "	
	Lu	0.020	" "	
4	Lu	0.020	Shaped-Outer	Spectral Index Measurements
	Cu	0.0105	" "	
	Lu	0.020	" "	
5	Cu	0.0105	0.272" Dia	Foil-to-Counter Geometry Corrections
6	Cu	0.0105	Shaped-Inner	
7	Cu	0.0105	0.272" Dia	
8	Cu	0.0105	Shaped-Outer	

TABLE 4

Description of Foil Materials and Gamma Counting Procedures

Foil		*Active*	*Thickness,*			*Counter*	*Counting Interval*
Detector	*Material*	*Wt %*	*inch*	*Activity*	*Half-Life*	*Bias, keV*	*After Irradiation*
Depl U	U	0.019 (^{235}U)	0.0032	^{239}Np	2.35 days	90-116	2.4 days
				FP	—	660	4-8 hours
Nat U	U	0.714 (^{235}U)	0.0043	^{239}Np	2.35 days	90-116	2-4 days
				FP	—		
^{63}Cu	Cu	69.1 (^{63}Cu)	0.0105	^{64}Cu	12.9 hours	400	4-18 days
^{176}Lu	Lu-Al	15 (Lu_2O_3)	0.020	^{177}Lu	6.8 days	30-250	2-4 days
^{235}U	U-Al	4.4 (^{235}U)	0.005	FP	—	200	4-8 hours

MEASUREMENT PROCEDURES

^{238}U Resonance Capture (ρ_{28})

This section describes the experimental techniques and corrections utilized for each type of measurement. Measurement results and comparison with computations are given in the section entitled "Comparison of Results."

ρ_{28} is an important parameter related to the resonance escape probability and, therefore, to the reactivity and ^{239}Pu production in uranium metal reactors. ρ_{28} is defined as the ratio of epicadmium to subcadmium ^{238}U captures in the fuel:

$$\rho_{28} = \frac{1}{^{238}U \text{ Cd Ratio} - 1}$$

Comparison of measured values of ρ_{28} with calculations yields useful information about the resonance treatment and slowing down models in the codes.

ρ_{28} was measured by the indirect or subtraction technique that permits the epicadmium component of the ^{238}U captures in the fuel to be determined without cadmium-covered ^{238}U foils. The capture cross sections of both ^{238}U and ^{63}Cu follow the 1/v law closely in the subcadmium region. Thus, the subcadmium ^{63}Cu activity in the fuel can be used to represent the subcadmium ^{238}U captures in the fuel if the two foil types are normalized in a thermal flux at the thermal column reference location. Then

$$^{238}U^{\text{Fuel}}_{\text{Sub-Cd}} = \left[{}^{63}Cu^{\text{Fuel}}_{\text{Sub-Cd}}\right]\left[\frac{^{238}U^{\text{Th Ref}}_{\text{Sub-Cd}}}{^{63}Cu^{\text{Th Ref}}_{\text{Sub-Cd}}}\right]\left[\frac{F_{\text{Cu Fuel}}}{F_{\text{Cu Foil}}}\right]\left[\frac{F_{\text{U Foil}}}{F_{\text{U Fuel}}}\right]$$

and

$$^{238}U^{\text{Fuel}}_{\text{Epi-Cd}} = {}^{238}U^{\text{Fuel}}_{\text{Total}} - {}^{238}U^{\text{Fuel}}_{\text{Sub-Cd}}$$

where

$^{238}U_{\text{Sub-Cd}}$ = subcadmium ^{238}U activity

$^{63}Cu_{\text{Sub-Cd}}$ = subcadmium ^{63}Cu activity

$^{238}U_{\text{Epi-Cd}}$ = epicadmium ^{238}U activity

$F_{\text{Cu Foil}}$, $F_{\text{U Foil}}$ = calculated thermal flux depression factor of the combined foil(s) and aluminum fission product guards at the foil site in the fuel (Appendix A)

$F_{Cu\ Fuel}$, $F_{U\ Fuel}$ = calculated thermal flux depression factor of a fictitious foil of fuel material corresponding to the thickness of the foil(s) and fission product guards at the foil site in the fuel (Appendix A)

ρ_{28} is calculated from

$$\rho_{28} = \frac{f\left[{}^{238}U^{Fuel}_{Epi\text{-}Cd}\right]}{\left[\frac{F_{U\ Fuel}}{(F_{U\ Foil})^2}\right]\left[{}^{238}U^{Fuel}_{Sub\text{-}Cd}\right]}$$

where

f = small correction (f_{inner} = 0.99; f_{outer} = 0.98) to account for the increase in ^{238}U resonance capture caused by the 1-mil gap at the interface of the foils and the fuel where aluminum was placed to prevent fission product contamination of the foils (Appendix B)

The ^{63}Cu cadmium ratio in the fuel is obtained from the bare copper foils in the fuel and 0.272-inch-diameter copper foils placed in a small cadmium pill box in the fuel. A direct measurement of the ^{238}U cadmium ratio with cadmium-covered ^{238}U would require a large cadmium-enclosed section to completely contain the foil in parent material. Thus, the indirect technique has the advantage of reducing the effect of flux and spectrum distortion produced by cadmium.

Bare depleted and natural uranium metal foils were used to determine the total ^{238}U neutron captures in the uranium fuel at each SE lattice pitch. Identical bare foils were simultaneously irradiated at the thermal reference position to normalize the subcadmium ^{238}U captures. The relative number was determined by counting the 2.3-day activity of

$$^{239}Np \xrightarrow[2.33\ d]{(\beta,\gamma)} {}^{239}Pu$$

produced from ^{238}U by

$$^{238}U \xrightarrow{(n,\gamma)} {}^{239}U \xrightarrow[23.3\ min]{(\beta,\gamma)} {}^{239}Np$$

The ^{239}Np gamma activities and the K_α and K_β x-rays were counted by NaI scintillators biased to accept energies in the interval from 90 to 116 keV. A simultaneous count at an integral bias of 500 keV was used to correct for the fission product contribution to the counting rate in the 90-116 keV energy window (~2% correction for depleted (0.019 wt %) uranium foils; ~10% correction for natural uranium foils). No gamma rays of energy greater than 430 keV were observed in the decay of ^{239}Np; thus, events having a minimum energy loss of 500 keV provide a measure of the fission activity. Details of the fission product correction are given in Appendix C. No systematic differences were noted in the ^{238}U capture activities deduced from the natural and depleted uranium foil types.

The ^{239}Np counting data were obtained in the time interval from 2 to 4 days after irradiation to maximize the 2.3-day ^{239}Np decay activity relative to the background fission product activity in the 90-116 keV window.

The usual corrections were made to the uranium foil-counting rates for room background, spontaneous decay background, counter deadtimes, and foil weight. The following additional corrections were made:

- Foil thickness correction to account for the difference in γ-ray self-attenuation between the 4.3-mil-thick natural uranium and the 3.2-mil-thick depleted uranium foils (Appendix D).

- Axial elevation correction to reduce the foil activities to a common elevation (Appendix E).

Bare and cadmium-covered copper foils were irradiated in the fuel to determine the subcadmium ^{63}Cu activity. Identical bare copper foils were simultaneously irradiated at the thermal reference to provide the normalization for the ρ_{28} measurement. The 500-keV annihilation gammas associated with the positron emission from ^{64}Cu were counted at an integral bias of 400 keV. The data were obtained beginning about 4 hours after irradiation when contribution from the 5.1-minute ^{66}Cu activity was negligible.

An auxiliary experiment was performed to obtain a factor of 1.088 to correct the average epicadmium specific activity of the two 0.272-inch-diameter × 0.0105-inch-thick copper foils used in the cadmium pill box in the fuel to the equivalent epicadmium specific activity for a single 0.500-inch-diameter × 0.0105-inch-thick copper foil under 30 mils of cadmium (dimensionally similar to the arc-shaped bare copper foils contained in the fuel). This correction simultaneously establishes the effective cadmium cutoff energy for the ρ_{28} measurement at 0.625 eV corresponding to 30 mils

of cadmium in slab geometry and isotropic flux with a 1/E energy dependence. The factor was determined experimentally by irradiating foils in both geometries under cadmium on a spinner in the center of the SP reactor. The resonance shielding effects of the lutetium and ^{235}U foils included with the copper foils in the cadmium pill boxes in the fuel were similarly accounted for by including them in this auxiliary experiment.

^{238}U Fast Fission (δ_{28})

Fast fission in ^{238}U can contribute significantly to the reactivity of lattices of plutonium-producing assemblies at low moderator-to-fuel ratios. The measurable quantity in any definition of the fast fission effect is δ_{28} defined as the ratio of the fission captures in ^{238}U to the fission captures in ^{235}U of the fuel. δ_{28} is used as one of the diagnostic parameters for direct comparison with lattice cell calculations.

The determination of δ_{28} requires the measurement of the fission rates in samples of ^{238}U and ^{235}U in the fuel elements of the reactor lattice. In practice, δ_{28} is obtained by irradiating small paired natural and depleted uranium foils in the fuel and then determining the number of fissions that have occurred from the fission product gamma activities produced. The fission product activities are measured by gamma counting with NaI scintillation counters. However, a one-to-one correspondence between the measured gamma-counting rates and the relative number of fissions represented in the foils does not exist because the fission product yields in ^{238}U and ^{235}U fissions are not identical.

The natural uranium foil fission product gamma activity is

$$A_N = K\,[AX(t) + BY(t)]$$

where

A = ^{235}U fissions in a natural uranium foil

B = ^{238}U fissions in a natural uranium foil

K = proportionality constant depending on counter bias, counter geometry, and counter efficiency

X(t) = ^{235}U fission product γ disintegrations per ^{235}U fission as a function of time t

Y(t) = ^{235}U fission product γ disintegrations per ^{238}U fission as a function of time t

The depleted uranium foil fission product gamma activity is

$$A_D = K\left(\frac{N_D}{N_N}\right)^{235} AX(t) + \left(\frac{N_D}{N_N}\right)^{238} BY(t)$$

where

N = atom density of the natural (N_N) or depleted (N_D) uranium foil

Defining $Y(t) = \frac{A_D}{A_N}$, $P(t) = \frac{X(t)}{Y(t)}$, and noting that $\delta_{28} \equiv \frac{B}{A}$, then

$$(\delta_{28})_{Nat} = P(t)\left[\frac{Y(t) - \left(\frac{N_D}{N_N}\right)^{235}}{\left(\frac{N_D}{N_N}\right)^{238} - Y(t)}\right]$$

This result applies to a measurement in natural uranium fuel with paired natural and depleted uranium foil detectors. When paired natural and depleted uranium foil detectors are used to measure δ_{28} in enriched uranium fuel, as was the case for the Type I and Type II fuel, it is necessary to scale the ^{235}U and ^{238}U atom densities by the expression

$$(\delta_{28})_{Enr} = (\delta_{28})_{Nat}\left[\frac{\left(\frac{N_{Enr}}{N_N}\right)^{238}}{\left(\frac{N_{Enr}}{N_N}\right)^{235}}\right]$$

where

N_N = atom density of natural uranium (N_N)

N_{Enr} = atom density of the enriched uranium fuel

P(t) is a time-dependent factor relating the ratio of measured foil gamma activities to the true fission ratio. P(t) depends on the fission product yields, foil thickness, exposure, and time after irradiation. P(t) usually is measured in an experiment using a double-chambered fission counter with thin films of depleted and natural uranium as fissioning elements and

with natural and depleted uranium foils contained between the fission chambers. During irradiation, the relative number of fissions occurring in the two films is determined by counting pulses from both chambers. After irradiation, the relative gamma activity of the foils is determined by counting with a scintillation counter.

Concurrent with the P(t) determination, a reference value can be measured by the simultaneous irradiation and counting of natural and depleted uranium foils for a particular reproducible reference geomtry with natural uranium fuel. Then δ_{28} measurements in the SE lattice with enriched fuel can be made by a simple simultaneous irradiation and counting of identical depleted and natural uranium foils in the reference position and in the SE lattice fuel; i.e.,

$$(\delta_{28})_{Fuel} = (\delta_{28})^{Nat}_{Ref} \left[\frac{\gamma(t) - \left(\frac{N_D}{N_N}\right)^{235}}{\left(\frac{N_D}{N_N}\right)^{238} - \gamma(t)}\right]\left[\frac{\left(\frac{N_D}{N_N}\right)^{238} - \gamma'(t)}{\gamma'(t) - \left(\frac{N_D}{N_N}\right)^{235}}\right]\left[\frac{\left(\frac{N_{Enr}}{N_N}\right)^{238}}{\left(\frac{N_{Enr}}{N_N}\right)^{235}}\right]$$

where

$\gamma'(t)$ = ratio of the specific gamma activity of the depleted uranium foil to the specific gamma activity of the natural uranium foil at the reference location

$\gamma(t)$ = ratio of the specific gamma activity of the depleted uranium foil to the specific gamma activity of the natural uranium foil in the lattice fuel

This technique was used for the measurements in the Type I and Type II fuel. The reference position consisted of two 1-inch diameter × 4-inch-long natural uranium slugs buried in a 20 × 20 × 28-inch block of graphite moderator. The graphite block was placed adjacent to the SP reactor where a well-thermalized neutron flux was incident. A pair of 1/2-inch diameter natural and depleted uranium foils identical in composition and thickness to those used in the lattice was placed in a shallow circular recess milled into the center face of one of the two 4-inch-long segments. This arrangement was easy to reproduce and eliminated edge effect errors due to foil misalignment. The $(\delta_{28})_{Fuel}$ values are based on a value of $(\delta_{28})^{Nat}_{Ref} = 0.076 \pm 0.001$ obtained by a direct measurement using the standard double fission chamber technique (Appendix F).

The $\gamma(t)$ ratios were obtained by counting the natural and depleted uranium foils at an integral bias of 500 keV during the time interval from 4 to 8 hours after the irradiation. Corrections for background, counter deadtime, and counter-foil geometry were included.

Modified Conversion Ratio (C^*)

The attainable fuel burnup in uranium-heavy water reactors is sensitive to the initial conversion ratio, i.e., the number of ^{239}Pu atoms produced per ^{235}U atom destroyed in fresh fuel. An accurate knowledge of this quantity is important in predicting the fuel economy. An easily measured parameter closely related to the initial conversion ratio is the modified conversion ratio,

$$C^* = \frac{\Sigma_a(238)}{\Sigma_{Fiss}(235)}$$

defined as ^{238}U (n,γ) absorptions normalized to ^{235}U total fissions. C^* is readily obtained from the neutron balance edit of the RAHAB code.

C^* is determined by the relative ^{235}U fission rates and the relative ^{238}U (n,γ) absorption rates in natural uranium and depleted uranium foils irradiated simultaneously in the SE lattice and in a pure thermal flux at the SE thermal column reference position:

$$C^* = \left[\frac{\Sigma_a(238)}{\Sigma_{Fiss}(235)}\right]^{Fuel}_{Th\ Ref} \cdot \frac{\left[^{239}Np\ Prod\right]_{Fuel}}{\left[^{239}Np\ Prod\right]_{Th\ Ref}} \cdot \frac{\left[^{235}U_{Fiss}\right]_{Th\ Ref}}{\left[^{235}U_{Fiss}\right]_{Fuel}}$$

where

$$[\Sigma_a(238)]^{Fuel}_{Th\ Ref} = N^{Fuel}_{238}\ g\sigma_a(238)$$

$$[\Sigma_{Fiss}(235)]^{Fuel}_{Th\ Ref} = N^{Fuel}_{235}\ g\sigma_f(235)$$

Constants used for the determination of C^* are given in Table 5.

TABLE 5

Constants Used in C^* Determination

	^{238}U	^{235}U
N, atoms/cc		
Type I Fuel	4.742×10^{22}	4.166×10^{20}
Type II Fuel	4.729×10^{22}	5.328×10^{20}
g	1.0017	0.9759
σ_a, barns	2.71	—
σ_f, barns	—	577

The ^{239}Np production ratios were obtained from the relative ^{239}Np activities of the natural and depleted uranium foils. The relative ^{235}U fission rates were obtained from the same natural and depleted uranium foils used to determine the ^{239}Np production ratios. The fission product gamma activities induced in the foils from ^{235}U and ^{238}U fissions were measured in the time interval from 4 to 6 hours after irradiation by using NaI scintillation counters biased at 660 keV. The fission product gamma activities of the natural and depleted foils are given by

$$A_N = A_{235} + A_{238}$$

$$A_D = \left(\frac{N_D}{N_N}\right)^{235} A_{235} + \left(\frac{N_D}{N_N}\right)^{238} A_{238}$$

where

A_N, A_D = natural (N) or depleted (D) uranium foil activity per 238 atom

A_{235}, A_{238} = ^{235}U or ^{238}U fission product component of the natural uranium foil activity per 238 atom

N_N, N_D = natural (N) or depleted (D) foil atom densities

The ^{235}U fission component was obtained from the paired natural and depleted foil activities by

$$A_{235} = \frac{A_N - \left(\frac{N_N}{N_D}\right)^{238} A_D}{1 - \Delta}$$

where

$$\Delta = \left(\frac{N_D}{N_N}\right)^{235} \cdot \left(\frac{N_N}{N_D}\right)^{238}$$

The ^{235}U fission component, A_{235}, was corrected for flux peaking at the paired natural depleted uranium foil site in the fuel by

$$(A_{235})_{Corr} = \frac{F_{Fuel}}{F_{Foil}} \cdot A_{235}\left[\frac{^{235}U\ Cd\ Ratio - 1}{^{235}U\ Cd\ Ratio}\right] + A_{235}\left[\frac{1}{^{235}U\ Cd\ Ratio}\right]$$

where

$\frac{F_{Fuel}}{F_{Foil}}$ = calculated ratio of thermal flux depression factors to correct the subcadmium ^{235}U fission product activity for flux peaking at the foil site in the fuel (Appendix A)

Thermal Neutron Spectral Index (*R*)

Reactivity effects in a D_2O-moderated uranium reactor are sensitive to the thermal energy spectrum of the neutron flux in the fuel. The activation ratio of subcadmium captures in ^{176}Lu to subcadmium captures in ^{63}Cu within the lattice cell is a sensitive parameter related to the energy distribution of the thermal neutron flux because the cross section of ^{176}Lu contains a resonance at 0.142 eV and ^{63}Cu is a 1/v detector. Normalization to the same ratio in a pure Maxwellian spectrum at the thermal reference provides a useful spectral index related to the thermal neutron hardening in the lattice cell. For direct comparison with experiment, the activation ratio is readily obtained from the FOILED edit of the RAHAB code, and the thermal reference ratio can be calculated from the Maxwellian spectrum and the ^{63}Cu and ^{176}Lu cross sections (Appendix G).

The spectral index measurements were made by simultaneous irradiation of bare and cadmium-covered lutetium-copper-lutetium foil sandwiches in the lattice cell and bare foil sandwiches in the thermal reference:

$$R = \frac{g_{Lattice}}{g_{Th\ Ref}} = \left[\frac{^{176}Lu}{^{63}Cu}\right]_{Sub\text{-}Cd}^{Fuel} \Big/ \left[\frac{^{176}Lu}{^{63}Cu}\right]_{Sub\text{-}Cd}^{Th\ Ref}$$

Arc-shaped foils were used in the fuel, and 0.272-inch-diameter foils were used on the fuel surfaces and in the moderator. Both foil types were represented at the thermal reference position. The 500-keV annihilation gammas from the positron decay of ^{64}Cu were counted with NaI scintillation counters biased at 400 keV beginning about 3 hours after irradiation. The ^{177}Lu was counted during the interval from 2 to 7 days after irradiation either with an integral bias setting of 30 keV or in a 30-250 keV window.

^{235}U Fission Ratio (δ_{25})

δ_{25}, defined as the ratio of epicadmium to subcadmium ^{235}U fissions in the fuel, is a sensitive index testing the flux, spectrum, cross section, and resonance shielding treatments of this important isotope in the lattice.

The δ_{25} measurements were made by activating bare, arc-shaped ^{235}U-Al foils in the fuel and 0.272-inch-diameter foils under cadmium in the fuel. The fission product gamma activity was measured during the time interval from 2 to 4 hours after irradiation by using NaI scintillation counters biased at 200 keV. Relative foil weights were determined in an auxiliary activation experiment where the foils were uniformly irradiated in a thermal flux and the fission product activity was measured. Corrections for counter background, counter deadtime, spontaneous decay, axial elevation, and foil weight were applied.

δ_{25} was determined as

$$\delta_{25} = \frac{{}^{235}U\text{Fission}_{\text{Epi-Cd}}}{\frac{F_{\text{Fuel}}}{F_{\text{Foil}}}\left[{}^{235}U\text{Fission}_{\text{Total}} - {}^{235}U\text{Fission}_{\text{Epi-Cd}}\right]}$$

where

$\frac{F_{\text{Fuel}}}{F_{\text{Foil}}}$ = calculated ratio of thermal flux depression factors to correct the subcadmium ^{235}U fission product activity for flux peaking at the foil site in the fuel (Appendix A)

Intracell Flux Profiles

Accurate representation of the thermal neutron density distribution is essential for predicting the fission power distribution in the fuel and for providing a check on the treatment of thermal neutron diffusion in the cell. Intracell thermal neutron density profiles were determined from bare and cadmium-covered ^{63}Cu (1/v) foil activations. The subcadmium component was obtained by subtracting the epicadmium specific activity (after elevation correction) from the bare foil activity. Small thermal flux depression corrections were applied to account for the flux depression at the foil sites in the moderator and for flux peaking at the foil sites in the fuel.

Corrections for radial leakage were made to the experimental data in the moderator to correct the intracell profile to flat flux conditions for comparison with RAHAB calculations. These corrections consisted of dividing by $J_0(B_R r)$, where B_R^2 is the radial buckling of the SE, and r is the radial position of the foil. The B_R^2 values for each lattice were obtained by fitting gold pin activations at different radii in the SE to the $J_0(B_R r)$ function. Values of B_R^2 are summarized in Tables 6 and 7 and are discussed in the section on "Comparison of Results - Material Buckling."

TABLE 6

Summary of Radial Bucklings for Type I Lattices

Lattice Pitch, inches	B_R^2, m^{-2}
5.5	9.50
6.0	9.36
7.0	9.30
8.0	9.48

TABLE 7

Summary of Radial Bucklings for Type II Lattices

Lattice Pitch, inches	B_R^2, m^{-2}
6.35	8.50
7.0	9.06
8.08	9.36
9.25	9.17
14.0	9.20[a]

a. Estimated

Material Buckling (B_m^2)

The satisfactory prediction of reactivity for simple benchmark experiments is taken as the most important criterion in testing a reactor physics code and its associated nuclear data library.

Material bucklings were measured by flux-mapping techniques in the cylindrical exponential facility (SE). Radial and axial curvatures were determined independently and combined to obtain $B_m^2 = B_R^2 + B_z^2$, the material buckling equation.

The ratio of cadmium-covered to bare gold pin activations was determined throughout the exponential, so that regions where flux curvature was energy-dependent could be avoided.

A separate irradiation was made with a cadmium shutter between the critical source reactor (SP) and the SE, thereby eliminating from consideration photoneutrons resulting from the gamma field of the SP. The shutter correction also eliminated contributions from neutrons that originated in the SP and were reflected from walls into the SE.

Two methods of profiling were used to determine axial bucklings, depending on whether the material buckling was larger or smaller than the radial buckling:

- Exponential profiles ($B_m^2 > B_R^2$) were measured with a small, boron-lined, gamma-compensated, traveling ion chamber attached to a constant speed, vertical drive mechanism mounted on top of the SE tank. The ion chamber traversed the lattice inside a 7/8-inch-ID aluminum dry well. The output current and vertical position of the detector were continuously transmitted, and digitized current readings, taken at 2-cm intervels over a total distance of 60 cm, were transferred to computer data cards. The axial buckling was determined as the curvature of the best fit to the experimental data points by varying parameters in a hyperbolic cosine function. The perturbation of the flux shape from the traveling monitor itself was negligible.

- Cosine axial flux profiles ($B_m^2 > B_R^2$) were measured by irradiating gold pins of standardized shape and mass. The gold pins were arranged at 8-cm intervals on stringers of 70-cm length; three such stringers were used for each experiment. In such cases, the data were fitted to a cosine function. The gold pin activations were measured by using NaI scintillation counters and include background, decay, and counter deadtime corrections. The traveling monitor could not be used for these more reactive lattices because of the large perturbation induced by the ion chamber.

Both the traveling monitor guide tube and gold pin stringers were located near the centerline of the exponential tank. Previous experience has shown, however, that the axial buckling is independent of the radial positions at which the flux profile is measured, provided the edge of the SE is avoided.

Radial flux profiles were measured by irradiation of standardized gold pins. Pins were located at from 12 to 30 interstitial positions within a given horizontal plane, and 3 such arrays of pins at different elevations were included for each lattice pitch. The counting of the pin activations was similar to that described for the axial measurements. The measured radial flux shapes were fit to a J_o Bessel function to determine the radial buckling.

RAHAB CALCULATIONS

The experimental data were compared with calculations performed by the RAHAB code on an IBM 360 computer. RAHAB uses multigroup integral transport theory and a modified Nordheim resonance treatment to calculate lattice parameters, neutron distributions, and neutron reaction rates in individual, one-dimensional lattice cells. Extensive printout options allow direct comparisons of calculated and experimental quantities. Input to the code consists of a geometrical description of the reactor lattice cell and of cross section libraries for the various reactor materials. The most recent cross sections from the Evaluated Nuclear Data File (ENDF/B-IV) were used in the calculations.

COMPARISON OF RESULTS

Thermal Flux Profiles

The subcadmium copper activation profiles in the fuel and moderator are compared with RAHAB calculations in Figures 6 and 7. The experimental data and the RAHAB computation have been normalized to one another by requiring the volume-weighted activations in the fuel to equal the computed value. The agreement between calculations and experiments is good, indicating that RAHAB can be used for the prediction of the thermal flux and fission power distribution within the cell.

Spectral Index Profiles (R)

The comparisons of RAHAB-predicted spectral indices to the measured spectral indices are shown in Figures 8 and 9. RAHAB predicts the qualitative behavior of spectrum hardening but overestimates the magnitude of the effect not only in the fuel but also in the moderator. The discrepancy may be a result of an overestimate of the magnitude of the 1/E flux component near the 0.14-eV peak of the ^{176}Lu resonance. Experimental values of the spectral index in the fuel (R) as a function of lattice pitch are compared with calculation in Figures 10 and 11.

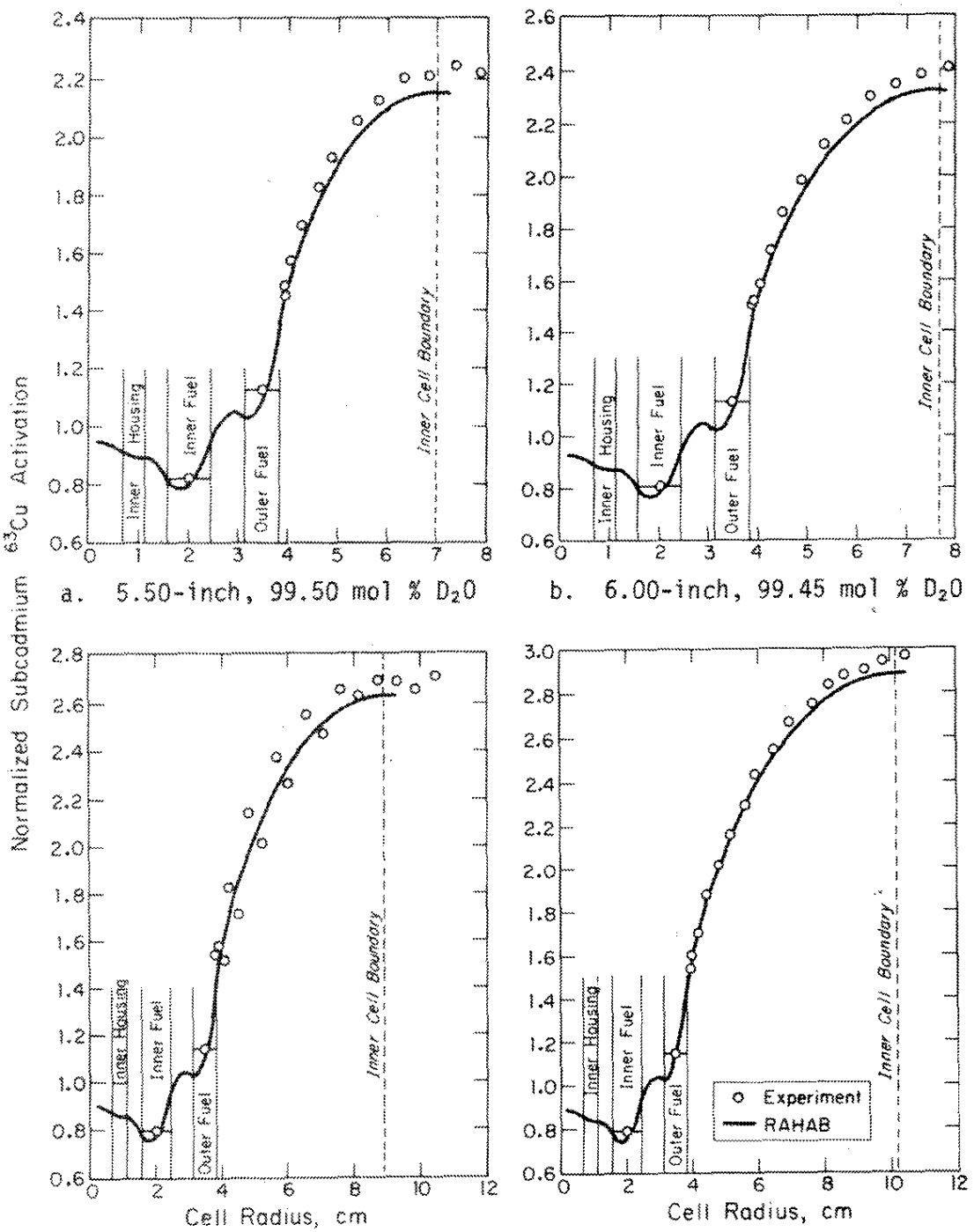

a. 5.50-inch, 99.50 mol % D_2O

b. 6.00-inch, 99.45 mol % D_2O

c. 7.00-inch, 99.41 mol % D_2O

d. 8.00-inch, 99.37 mol % D_2O

FIGURE 6. Intracell Subcadmium Copper Activation Profiles for Type I Fuel

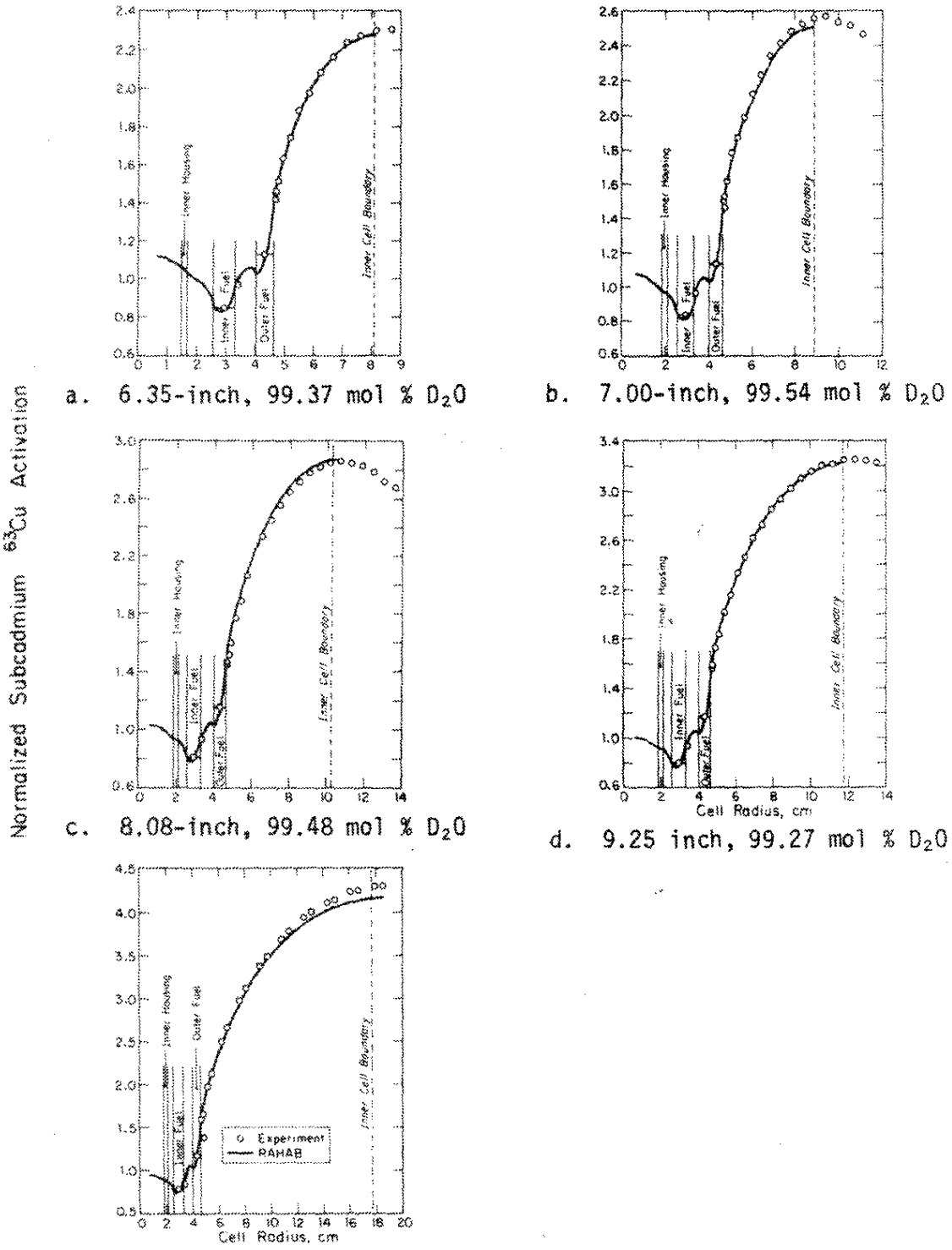

a. 6.35-inch, 99.37 mol % D_2O

b. 7.00-inch, 99.54 mol % D_2O

c. 8.08-inch, 99.48 mol % D_2O

d. 9.25 inch, 99.27 mol % D_2O

e. 14.00-inch, 99.14 mol % D_2O

FIGURE 7. Intracell Subcadmium Copper Activation Profiles for Type II Fuel

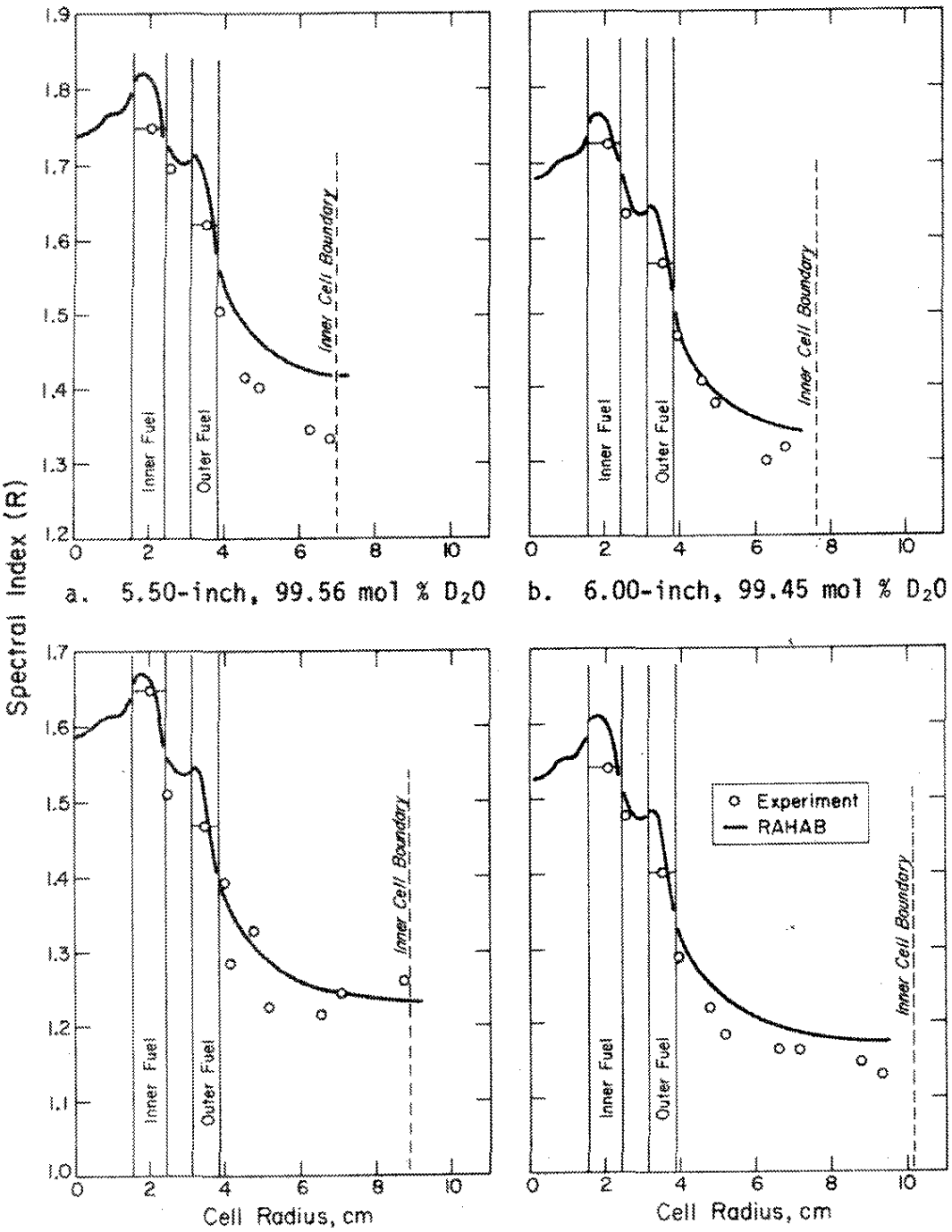

FIGURE 8. Intracell Spectral Index Profiles for Type I Fuel

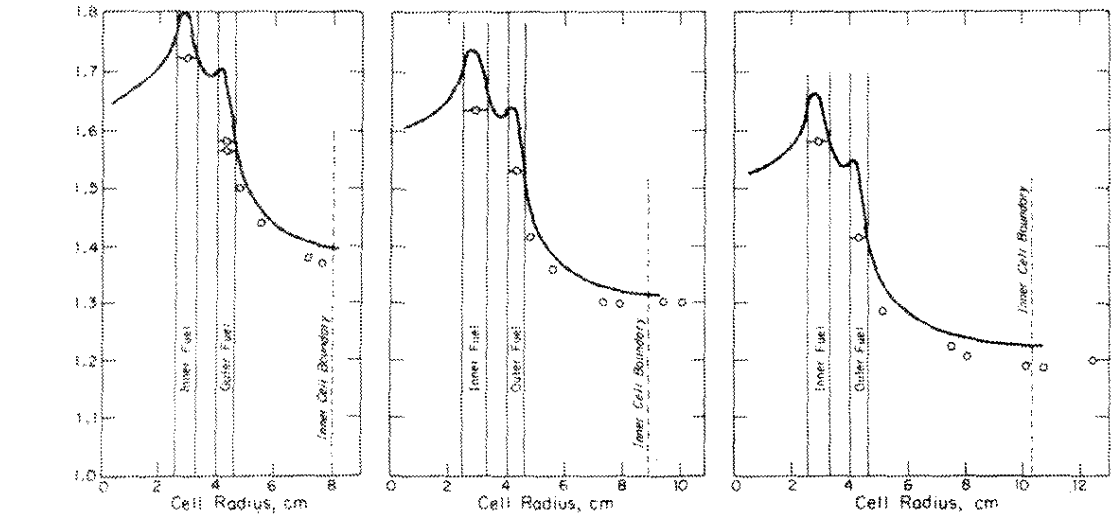

a. 6.35-inch, 99.37 mol % D_2O

b. 7.00-inch, 99.54 mol % D_2O

c. 8.08-inch, 99.48 mol % D_2O

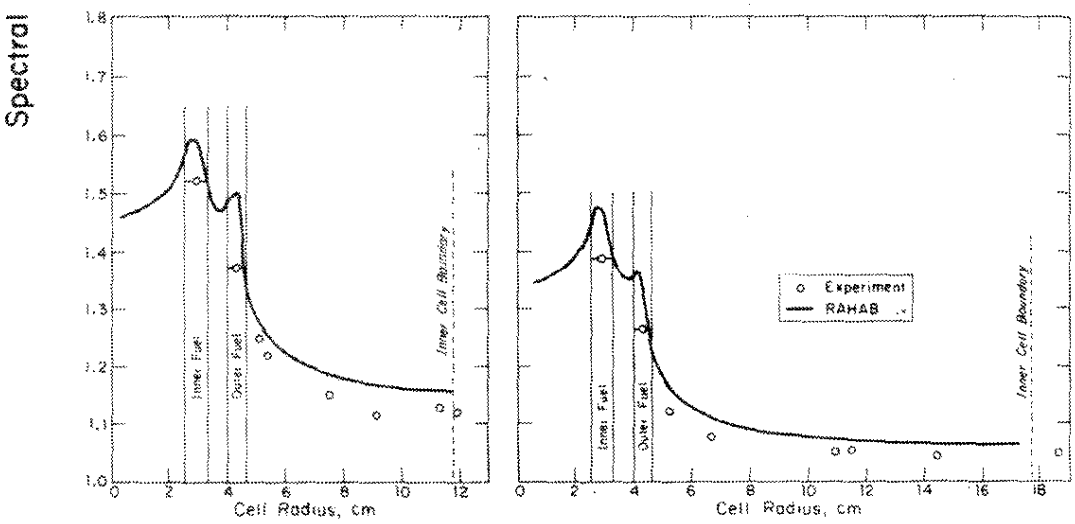

d. 9.25-inch, 99.27 mol % D_2O

e. 14.00-inch, 99.14 mol % D_2O

FIGURE 9. Intracell Spectral Index Profiles for Type II Fuel

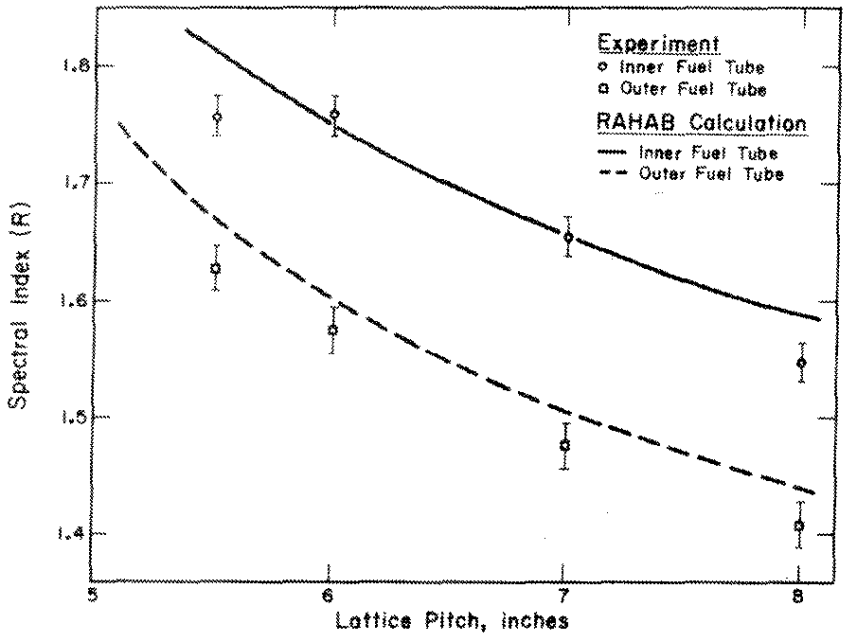

FIGURE 10. Comparison of Measured and Calculated R for Type I Fuel at 99.75 mol % D_2O

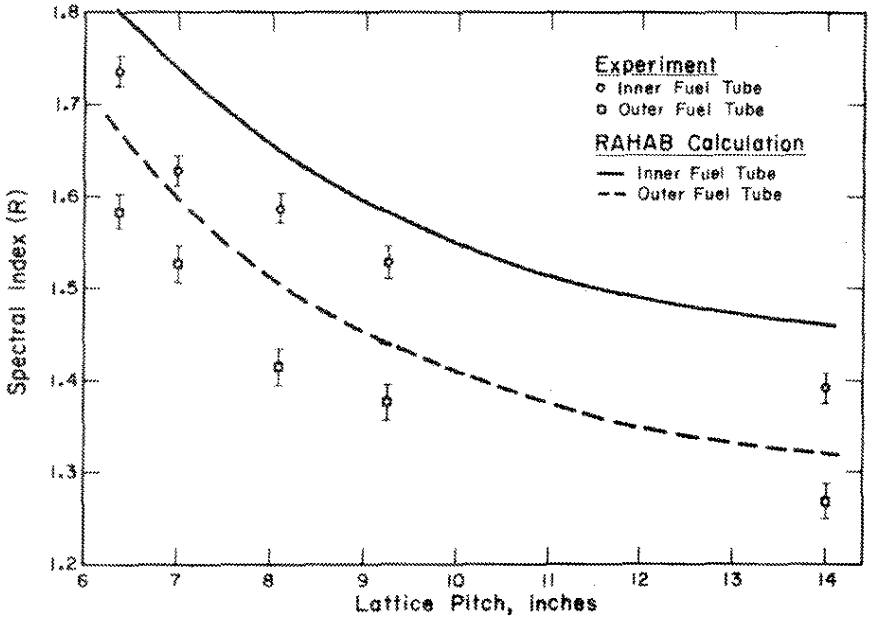

FIGURE 11. Comparison of Measured and Calculated R for Type II Fuel at 99.75 mol % D_2O

^{238}U Fast Fission (δ_{28})

RAHAB underestimates δ_{28} for both fuel types by about 11% for the inner fuel and about 7% for the outer fuel. The comparisons are shown in Figures 12 and 13. These results are consistent with an observation by Kemshell[9] that fast fission ratios are significantly (~10%) underpredicted for most lattices. The discrepancy may be a result of error(s) in the ^{238}U fast fission cross section, the ^{238}U inelastic cross section, and the ^{235}U and ^{239}U fission neutron spectra.

^{235}U Fission Ratio (δ_{25})

RAHAB overpredicts the ratio of epicadmium to subcadmium ^{235}U fissions (δ_{25}). For both Type I and Type II fuel, δ_{25} (inner fuel) is overestimated by about 23% on average, and δ_{25} (outer fuel) is overestimated by about 14% (Figures 14 and 15). This magnitude of discrepancy is not likely a result of any small difference in the thermal cutoff energy between calculation and experiment. The discrepancy is believed to be a result of the resonance treatment method used in RAHAB. The calculation treats the ^{235}U resonances individually and neglects the effects of overlapping of ^{238}U and neighboring ^{235}U resonances.

^{238}U Resonance Capture (ρ_{28})

Measured and calculated ρ_{28} are compared in Figures 16 and 17. For Type I fuel, ρ_{28} (outer fuel) is slightly overpredicted by about 4% average, and ρ_{28} (inner fuel) is consistently overpredicted by about 22% on average. For Type II fuel, ρ_{28} (outer fuel) is overpredicted by about 10%, and ρ_{28} (inner fuel) is overpredicted by about 20%. These discrepancies suggest that epithermal ^{238}U neutron capture is being overpredicted by RAHAB. Any reduction of the epithermal ^{238}U capture cross sections to force agreement does not appear warranted by current differential cross section measurements; therefore, the major part of the discrepancies is most likely attributed to the resonance capture treatment by RAHAB.

Modified Conversion Ratio (C^*)

Comparison of measured and calculated C^* is summarized in Figures 18 and 19. RAHAB overestimates C^* (inner fuel) for both fuel types by about 8% and C^* (outer fuel) by about 1% for Type I fuel and about 4% for Type II fuel. Because C^* is dominated by thermal rather than resonance effects, the magnitude of disagreement in C^* between calculation and experiment is less than in ρ_{28}.

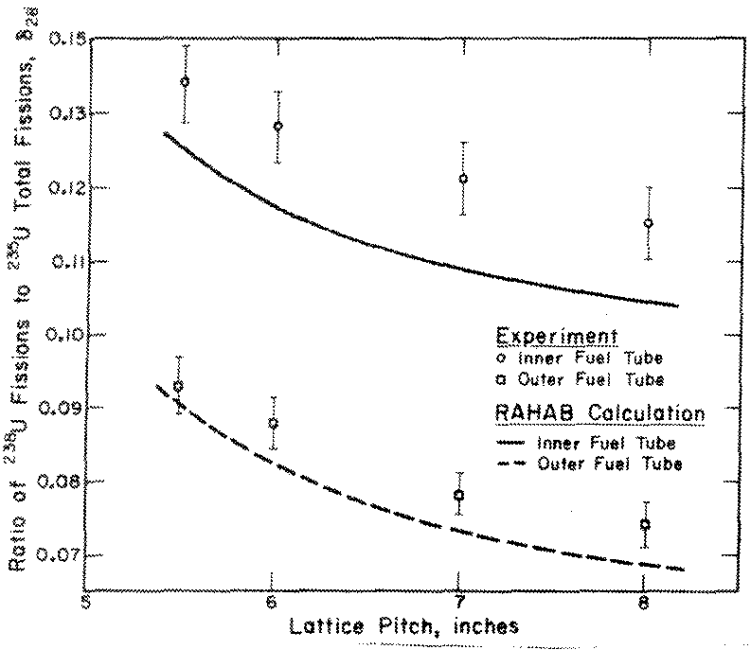

FIGURE 12. Comparison of Measured and Calculated δ_{28} for Type I Fuel at 99.75 mol % D_2O

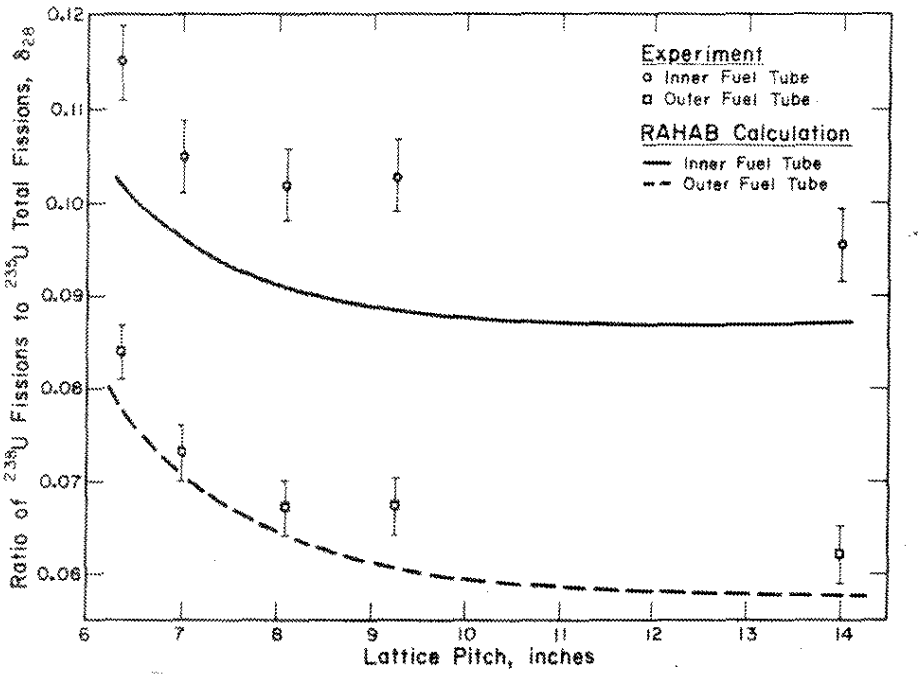

FIGURE 13. Comparison of Measured and Calculated δ_{28} for Type II Fuel at 99.75 mol % D_2O

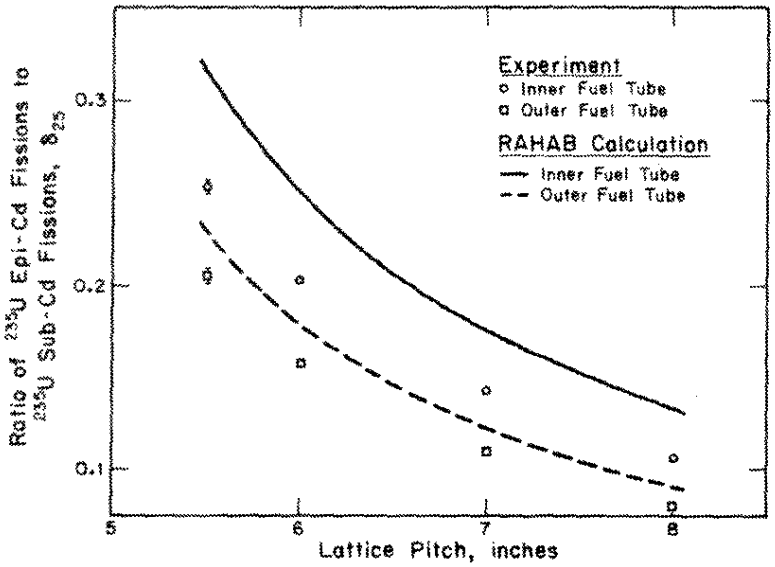

FIGURE 14. Comparison of Measured and Calculated δ_{25} for Type I Fuel at 99.75 mol % D_2O

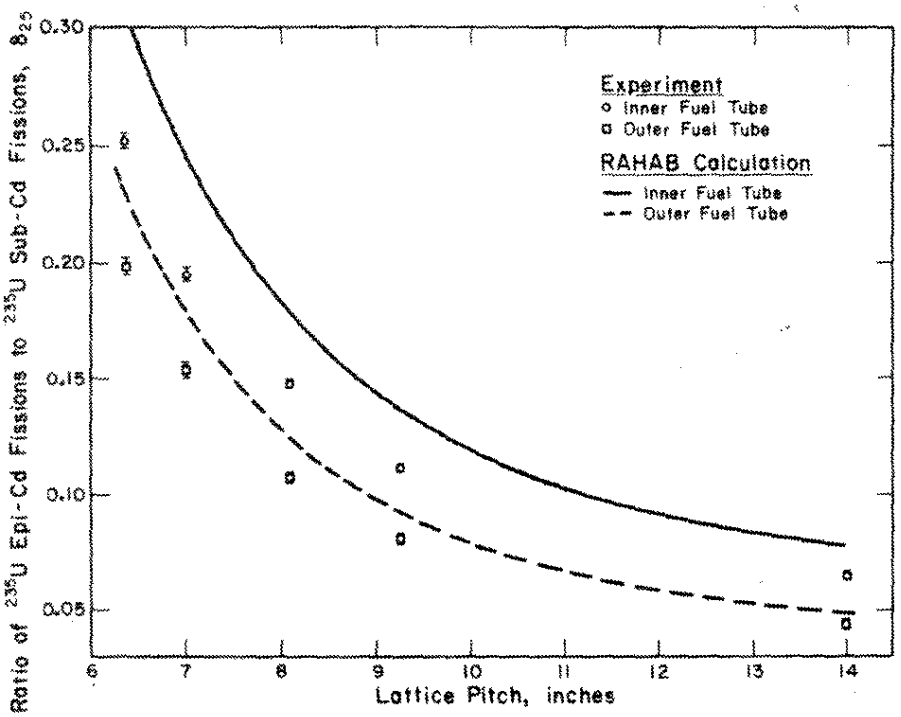

FIGURE 15. Comparison of Measured and Calculated δ_{25} for Type II Fuel at 99.75 mol % D_2O

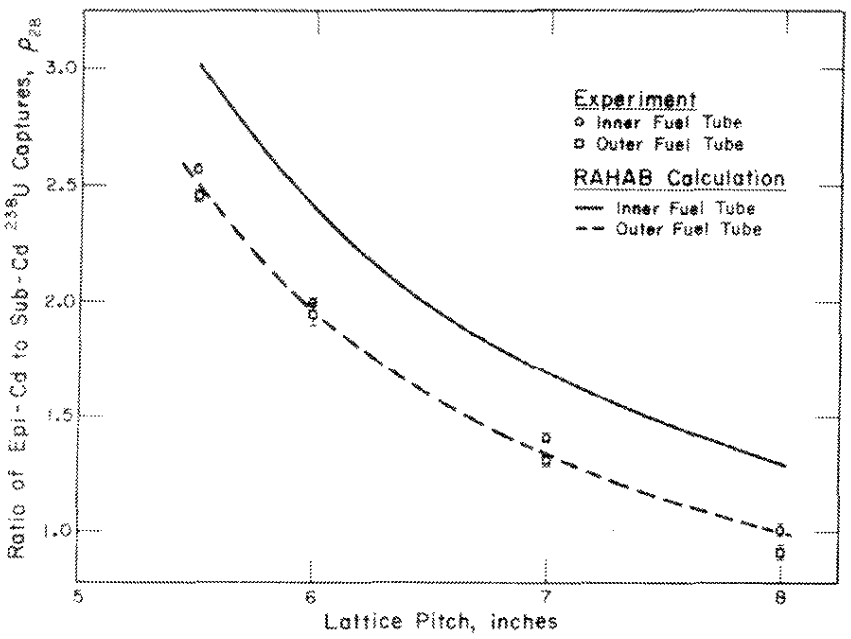

FIGURE 16. Comparison of Measured and Calculated ρ_{28} for Type I Fuel at 99.75 mol % D_2O

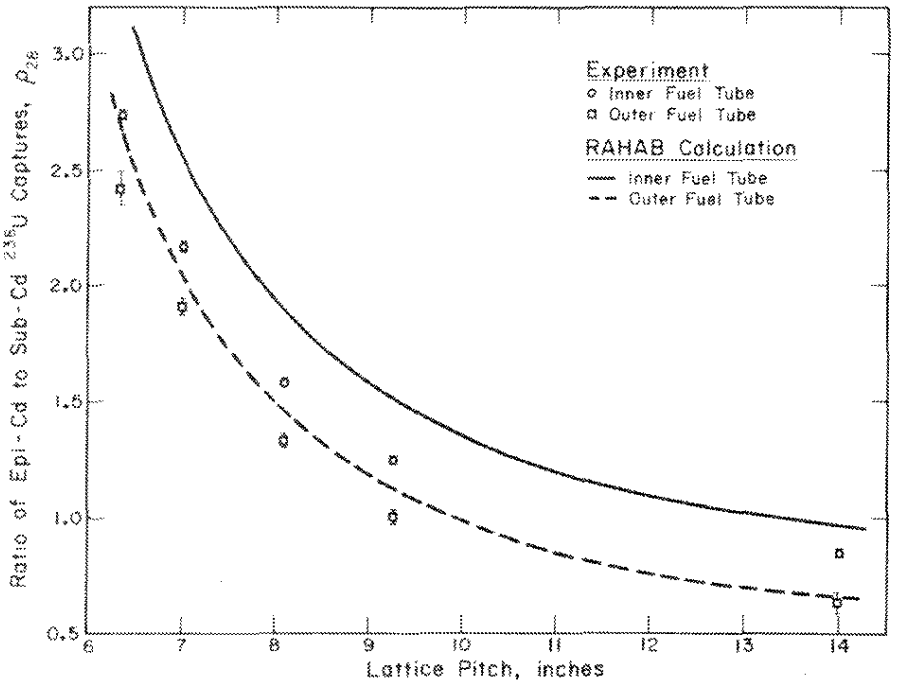

FIGURE 17. Comparison of Measured and Calculated ρ_{28} for Type II Fuel at 99.75 mol % D_2O

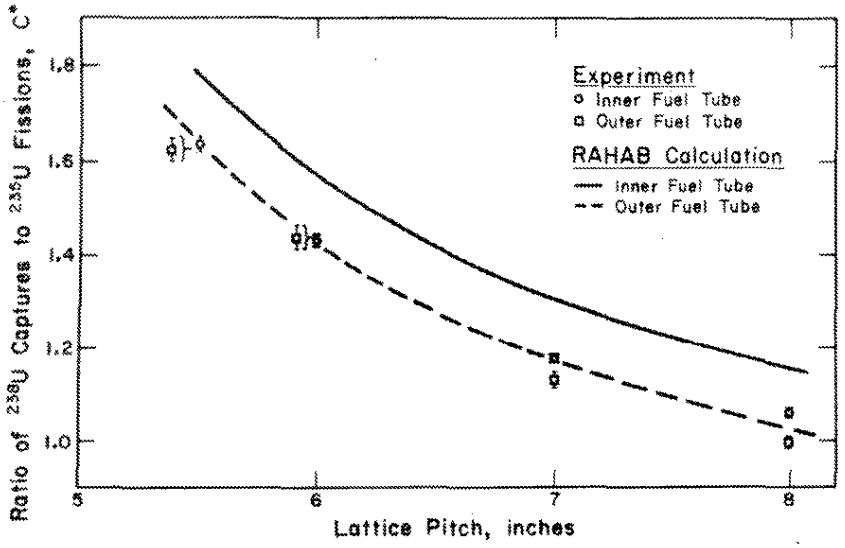

FIGURE 18. Comparison of Measured and Calculated C* for Type I Fuel at 99.75 mol % D_2O

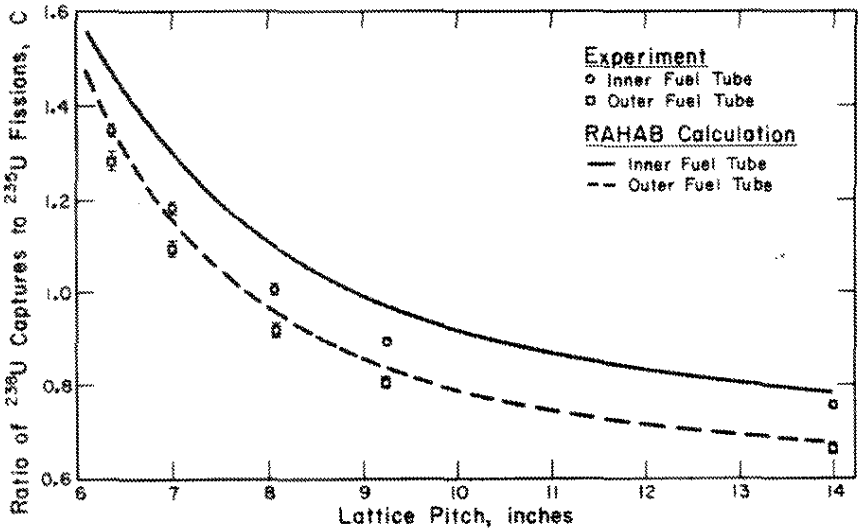

FIGURE 19. Comparison of Measured and Calculated C* for Type II Fuel at 99.75 mol % D_2O

Material Buckling (B_m^2)

The results of the buckling measurements for both fuel types are given in Tables 8 and 9. Bucklings and k_{eff} values calculated using the integral transport theory code RAHAB with ENDF/B-IV cross sections also are included. The calculated material bucklings are consistently lower than experiment for both fuel types (Figures 20 and 21). The discrepancies correspond to errors in k_{eff} of from 4 to 8% with the largest disagreements at the lower pitches (increasing fuel-to-moderator ratio).

For both the axial and radial measurements, the standard deviation in flux was approximately 0.5%. This uncertainty in flux induces an uncertainty in buckling that is dependent on the magnitude and nature of the curvature. The standard deviation in axial buckling ranges from 0.10 to 0.20 m^{-2}; and for the radial buckling, the range is from 0.20 to 0.35 m^{-2}. These statistical uncertainties in flux and buckling are primarily associated with uncertainties in gold pin mass, gold pin position, and position of fuel assemblies. Repetition of buckling measurements after unloading and reloading of fuel and pins indicates the bucklings can be reproduced to within 0.10 m^{-2}.

The major source of systematic error in these experiments is expected to be the application of exponential theory to a lattice. The detailed effects of this approximation on the buckling measurements have not been investigated. However, an SE buckling measurement was compared to a critical measurement of the same lattice. The test lattice was very similar to lattice Types I and II. The buckling of the test lattice as measured in the critical facility was lower than the SE value by 0.20 m^{-2}. No adjustment in the data of Tables 8 and 9 was made on the basis of this information; the error ranges in those tables reflect only the statistical uncertainties in the measurements. In all cases, however, the discrepancy between measured and calculated values of the material buckling are significantly larger than either the experimental uncertainties or the possible bias between critical and exponential measurements.

The radial bucklings for Type I and Type II fuels exhibit no regular or easily predictable dependence on lattice pitch. The explanation for this, as may be deduced from Figures 2 and 3, is that the effective core radius or alternately the geometry of the core leakage boundary for a given fuel type has no systematic dependence on lattice pitch.

TABLE 8

Comparison of Measured and Calculated Material Bucklings for Type I Fuel at 99.75 mol % D_2O

Lattice pitch, inches	5.50	6.00	7.00	8.00
Axial buckling, m^{-2}	-14.42 ±0.20	-8.94 ±0.20	-2.53 ±0.10	-0.28 ±0.10
Radial buckling, m^{-2}	9.50 ±0.30	9.36 ±0.30	9.30 ±0.25	9.48 ±0.20
Material buckling, m^{-2}				
Measured	-4.92 ±0.36	0.42 ±0.36	6.77 ±0.27	9.20 ±0.22
RAHAB-ENDF/B-IV	-10.95	-4.57	2.88	6.30
k_{eff} (RAHAB-ENDF/B-IV)	0.921	0.933	0.942	0.951

TABLE 9

Comparison of Measured and Calculated Material Bucklings for Type II Fuel at 99.75 mol % D_2O

Lattice pitch, inches	6.35	7.00	8.08	9.25
Axial buckling, m^{-2}	-5.72 ±0.20	-1.36 ±0.20	2.46 ±0.10	4.01 ±0.10
Radial buckling, m^{-2}	8.50 ±0.22	9.06 ±0.22	9.36 ±0.20	9.17 ±0.20
Material buckling, m^{-2}				
Measured	2.78 ±0.30	7.70 ±0.30	11.82 ±0.22	13.18 ±0.22
RAHAB-ENDF/B-IV	-2.64	3.24	8.57	10.81
k_{eff} (RAHAB-ENDF/B-IV)	0.928	0.940	0.951	0.960

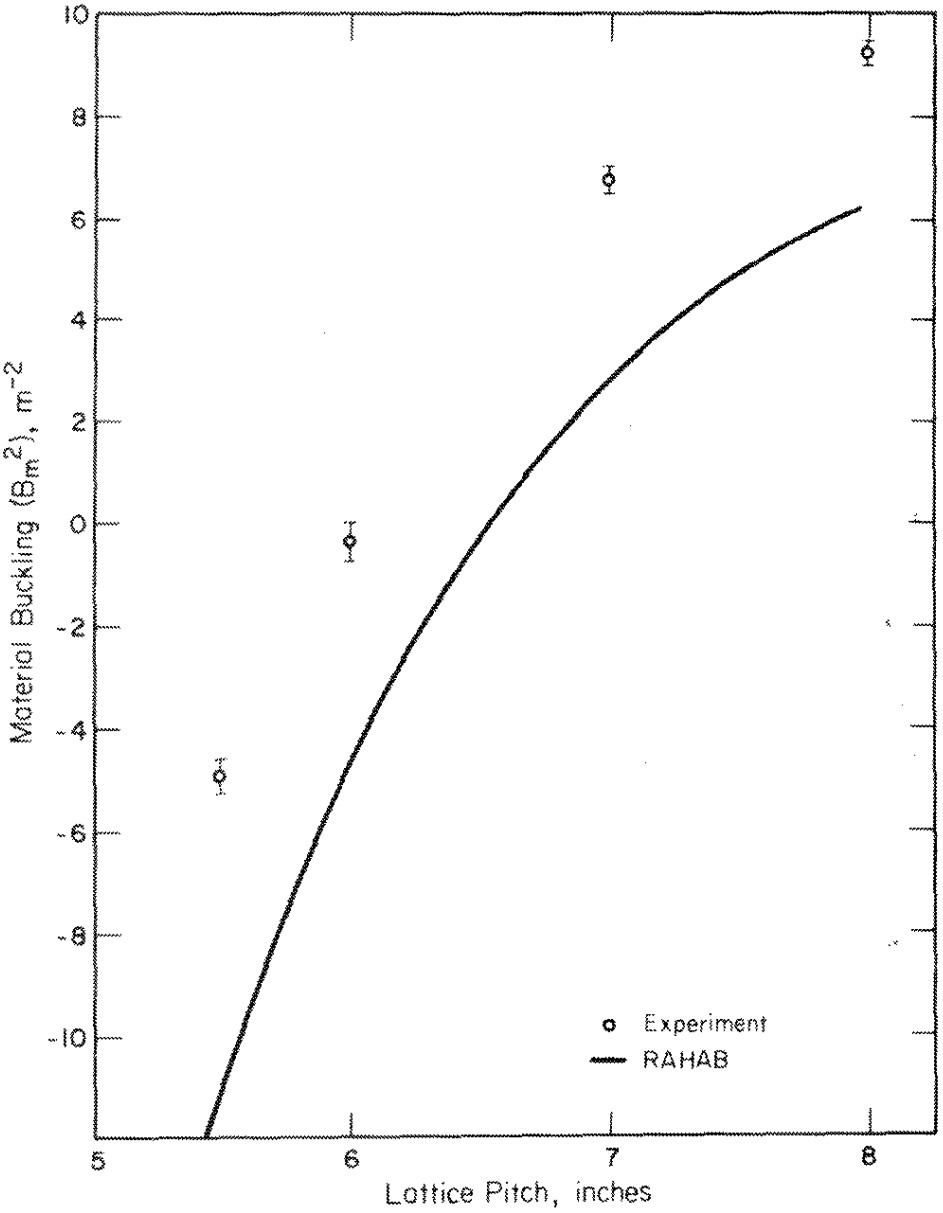

FIGURE 20. Comparison of Measured and Calculated B_m^2 for Type I Fuel at 99.75 mol % D_2O

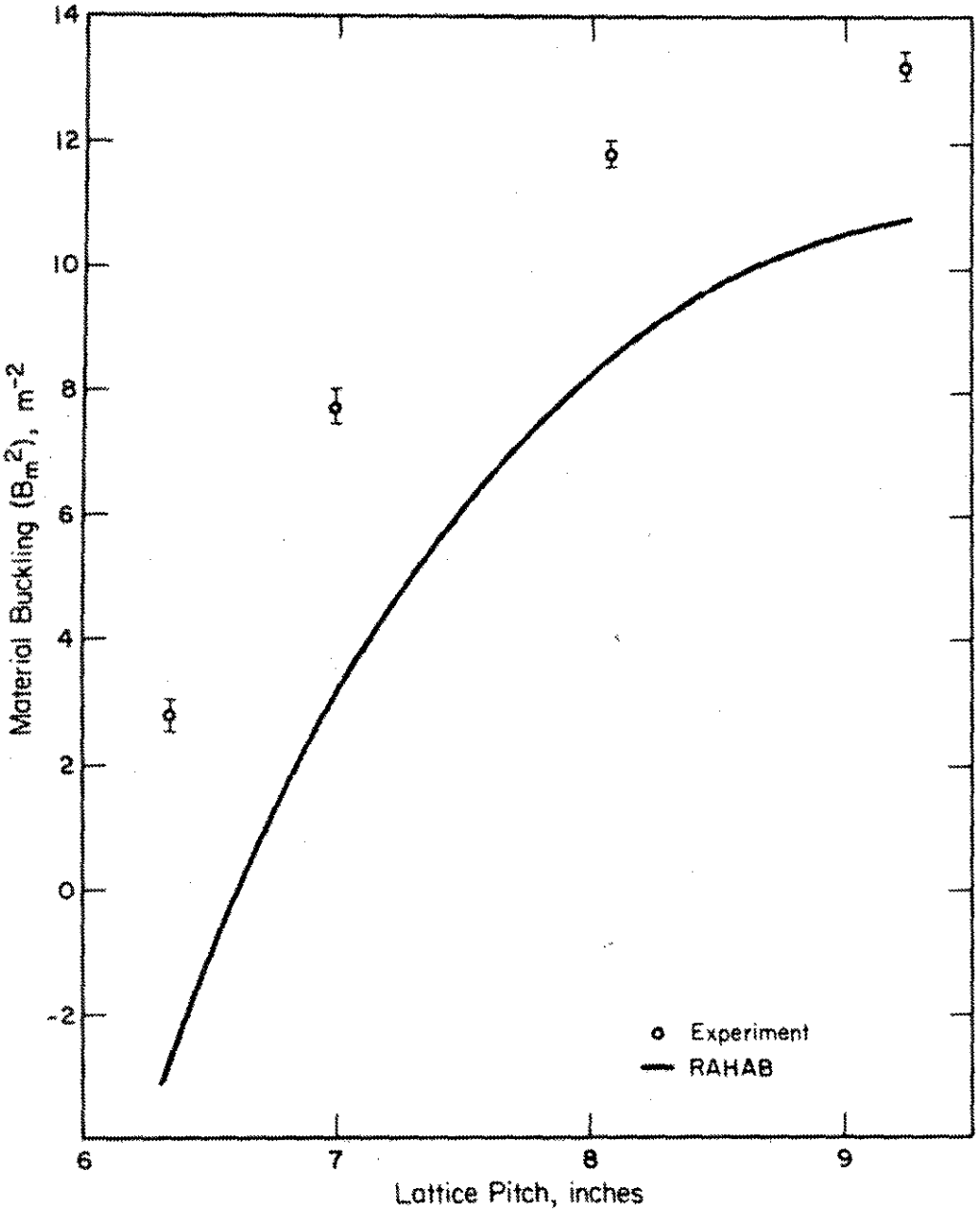

FIGURE 21. Comparison of Measured and Calculated B_m^2 for Type II Fuel at 99.75 mol % D_2O

Conclusions

In general, the discrepancies in the reaction rate measurements between experiment and RAHAB do not show a pitch dependence (Tables 10 and 11). Also, the calculations do less well in predicting inner fuel parameters.

The overprediction of ρ_{28}, C*, and δ_{25} and the underprediction of δ_{28} are consistent with the underprediction of material buckling and k_{eff} by RAHAB. The magnitudes of the discrepancies are larger than uncertainties in input cross sections, experimental uncertainties, or possible systematic bias in the experimental methods. The most probable source of discrepancy is the theoretical treatment of resonance capture in the RAHAB calculations.

The detailed reaction rate parameters and material bucklings presented here constitute a set of data that should complement existing benchmark D_2O lattice data. Coaxial tube fuel assemblies, such as Type I and Type II, provide a more-detailed set of reaction rate data for comparison of calculation to experiment than is possible for simple rod lattices. Also, the Type I and Type II fuel at the lattice pitches considered represent fuel-to-moderator ratios that are significantly larger than for other measured D_2O lattices. For example, the 6.35-inch-pitch Type II lattice has a ratio of uranium to deuterium (U/D) that is a factor of ten larger than that of the highest U/D ratio of the MIT rod lattices.[5] The significance of this is that the Type I and Type II lattices enhance the relative number of captures in ^{238}U and thus present a more rigorous test of calculational methods for resonance capture.

EXPERIMENTAL REPRODUCIBILITY

The parameter measurements at the 6.35-inch pitch with Type II fuel were repeated (Experiment 6) at the end of the experimental program to check reproducibility. The 6.35-inch-pitch case was chosen because, at this high fuel-to-moderator ratio, resonance capture effects are accentuated and geometry reproducibility is more critical. The earlier measurements (Experiment 3) had been completed with a D_2O purity of 99.37 mol %, although the purity at the time of Experiment 6 was 99.13 mol %. Small calculated corrections were used to convert the results to a common purity of 99.75 mol %. The comparison is summarized in Table 12. The measurements were duplicated within a 2σ range (values of σ given in Table 11).

TABLE 10

Comparison of Measured and Calculated Reaction Rate Parameters for Type I Fuel at 99.75 mol % D_2O

		Inner Fuel				*Outer Fuel*				*Assembly Avg.*		
Parameter	*Pitch*	*Expt.*	*Std. Dev.*	*Calc.*	*Calc./ Expt.*	*Expt.*	*Std. Dev.*	*Calc.*	*Calc./ Expt.*	*Expt.*	*Calc.*	*Calc./ Expt.*
ρ_{28}	5.5	2.550	±0.019	3.008	1.180	2.432	±0.016	2.504	1.030	2.472	2.676	1.083
	6.0	1.971	±0.013	2.396	1.216	1.928	±0.050	1.952	1.012	1.942	2.102	1.082
	7.0	1.388	±0.012	1.687	1.215	1.291	±0.028	1.330	1.030	1.323	1.448	1.094
	8.0	1.041	±0.016	1.299	1.248	0.905	±0.034	0.998	1.103	0.949	1.097	1.156
				Avg	1.215			Avg	1.044			
C*	5.5	1.656	±0.016	1.777	1.073	1.645	±0.024	1.634	0.993	1.649	1.684	1.021
	6.0	1.447	±0.014	1.570	1.085	1.451	±0.025	1.425	0.982	1.449	1.475	1.018
	7.0	1.190	±0.012	1.309	1.100	1.142	±0.017	1.170	1.025	1.158	1.217	1.051
	8.0	1.059	±0.011	1.154	1.090	0.998	±0.015	1.026	1.028	1.024	1.399	1.037
				Avg	1.087			Avg	1.007			
δ_{25}	5.5	0.254	±0.003	0.313	1.232	0.205	±0.004	0.229	1.117	0.222	0.257	1.158
	6.0	0.203	±0.002	0.249	1.227	0.157	±0.003	0.178	1.134	0.173	0.202	1.168
	7.0	0.142	±0.0015	0.174	1.225	0.109	±0.002	0.121	1.110	0.120	0.138	1.150
	8.0	0.105	±0.001	0.132	1.257	0.0787	±0.0015	0.0901	1.145	0.0874	0.104	1.190
				Avg	1.235			Avg	1.127			
δ_{28}	5.5	0.134	±0.005	0.125	0.933	0.0928	±0.004	0.0903	0.973	0.107	0.102	0.953
	6.0	0.128	±0.005	0.117	0.914	0.0878	±0.0035	0.0822	0.936	0.102	0.0943	0.925
	7.0	0.121	±0.005	0.109	0.901	0.0777	±0.003	0.0734	0.945	0.0921	0.0853	0.926
	8.0	0.115	±0.0045	0.104	0.904	0.0740	±0.003	0.0685	0.926	0.0876	0.0803	0.917
				Avg	0.913			Avg	0.945			
R	5.5	1.757	±0.017	1.811	1.031	1.628	±0.024	1.673	1.028			
	6.0	1.759	±0.017	1.749	0.994	1.575	±0.023	1.604	1.018			
	7.0	1.656	±0.016	1.655	0.999	1.477	±0.022	1.504	1.018			
	8.0	1.547	±0.015	1.590	1.028	1.407	±0.021	1.439	1.023			
				Avg	1.013			Avg	1.022			

TABLE II

Comparison of Measured and Calculated Reaction Rate Parameters for Type II Fuel at 99.75 mol % D_2O

		Inner Fuel				*Outer Fuel*				*Assembly Avg.*		
Parameter	*Pitch*	*Expt.*	*Std. Dev.*	*Calc.*	*Calc./ Expt.*	*Expt.*	*Std. Dev.*	*Calc.*	*Calc./ Expt.*	*Expt.*	*Calc.*	*Calc./ Expt.*
ρ_{28}	6.35	2.701	±0.026	3.235	1.198	2.387	±0.076	2.688	1.126	2.507	2.900	1.157
	7.00	2.145	±0.013	2.558	1.193	1.878	±0.034	2.058	1.096	1.979	2.248	1.136
	8.08	1.563	±0.013	1.896	1.213	1.311	±0.024	1.462	1.115	1.404	1.624	1.157
	9.25	1.229	±0.015	1.494	1.216	0.983	±0.029	1.113	1.132	1.073	1.253	1.168
	14.0	0.815	±0.019	0.945	1.160	0.611	±0.043	0.648	1.061	0.685	0.754	1.101
					Avg 1.196				Avg 1.106			
C*	6.35	1.341	±0.013	1.470	1.096	1.269	±0.020	1.340	1.056	1.305	1.391	1.066
	7.00	1.183	±0.012	1.289	1.090	1.094	±0.016	1.153	1.054	1.135	1.206	1.063
	8.08	1.006	±0.010	1.096	1.089	0.922	±0.014	0.962	1.043	0.959	1.013	1.056
	9.25	0.897	±0.009	0.972	1.084	0.810	±0.012	0.844	1.042	0.847	0.891	1.052
	14.0	0.755	±0.008	0.789	1.045	0.666	±0.010	0.678	1.018	0.702	0.718	1.023
					Avg 1.081				Avg 1.043			
δ_{25}	6.35	0.252	±0.003	0.307	1.218	0.199	±0.004	0.231	1.161	0.220	0.260	1.182
	7.00	0.195	±0.002	0.242	1.241	0.155	±0.003	0.177	1.142	0.170	0.201	1.182
	8.08	0.148	±0.0015	0.177	1.196	0.108	±0.002	0.125	1.157	0.123	0.144	1.171
	9.25	0.112	±0.001	0.137	1.223	0.0809	±0.0015	0.0938	1.159	0.0923	0.110	1.192
	14.0	0.0648	±0.001	0.0783	1.208	0.0441	±0.001	0.0504	1.143	0.0515	0.0603	1.171
					Avg 1.217				Avg 1.152			
δ_{28}	6.35	0.115	±0.004	0.102	0.887	0.0843	±0.003	0.0773	0.917	0.0962	0.0872	0.906
	7.00	0.104	±0.004	0.0962	0.925	0.0731	±0.003	0.0705	0.964	0.0850	0.0805	0.947
	8.08	0.102	±0.004	0.0909	0.891	0.0672	±0.003	0.0640	0.952	0.0801	0.0742	0.926
	9.25	0.103	±0.004	0.0884	0.858	0.0675	±0.003	0.0604	0.895	0.0805	0.0709	0.881
	14.0	0.0954	±0.004	0.0869	0.911	0.0620	±0.0025	0.0573	0.924	0.0741	0.0680	0.918
					Avg 0.894				Avg 0.930			
R	6.35	1.737	±0.017	1.800	1.036	1.586	±0.023	1.673	1.055			
	7.00	1.644	±0.016	1.734	1.055	1.539	±0.023	1.597	1.038			
	8.08	1.589	±0.016	1.649	1.038	1.419	±0.021	1.506	1.061			
	9.25	1.530	±0.015	1.585	1.036	1.378	±0.021	1.440	1.045			
	14.0	1.392	±0.014	1.459	1.048	1.267	±0.019	1.318	1.040			
					Avg 1.043				Avg 1.048			

TABLE 12

Experimental Reproducibility - Type II Fuel,
6.35-inch Pitch, 99.75 mol % D_2O

	ρ_{28}		C^*		δ_{25}		δ_{28}		R	
Experiment	*Inner*	*Outer*	*Inner*	*Outer*	*Inner*	*Outer*	*Inner*	*Outer*	*Inner*	*Outer*
3	2.724	2.400	1.346	1.281	0.251	0.196	0.104	0.0780	1.726	1.582
6	2.677	2.373	1.336	1.258	0.254	0.202	0.108	0.0773	1.716	1.556
3/6	1.018	1.011	1.007	1.018	0.988	0.970	0.963	1.009	1.006	1.017

APPENDIX A – THERMAL FLUX DEPRESSION FACTORS

Corrections were applied to the measured subcadmium foil activities to account for the thermal flux peaking (or depression) that occurred at foil sites in the fuel and moderator and to reduce the measured subcadmium activities to values for infinitely thin foil detectors. Thermal flux depression factors were used for this purpose. The thermal flux depression factor, F, is defined as the ratio of the specific activity of a finite thickness foil to that which an infinitely thin foil of the same material would have had under identical irradiation conditions. To correct for flux peaking in the fuel, the subcadmium activity of the foils in the fuel was multiplied by the ratio

$$\frac{F_{Fuel}}{F_{Foil}}$$

where

F_{Foil} = thermal flux depression factor of the combined foil(s) and aluminum fission product guards

F_{Fuel} = thermal flux depression factor of an equivalent thickness fictitious foil of fuel material

This ratio then corrects the actual average flux in the foil to the proper value corresponding to the average flux in the fuel. For foils in the moderator, the subcadmium activity was multiplied by the ratio

$$\frac{F_{D_2O}}{F_{Foil}} \approx \frac{1}{F_{Foil}} \quad \text{and} \quad F_{D_2O} \approx 1$$

The corrections were determined from the formalism of DP-817.[10] The model assumes an isotropic and monoenergetic neutron flux incident on a slab absorber within a cavity. The average flux depression within the slab is given by

$$F_{Slab} = \frac{1 - 2\,E_3(X)}{2X}$$

where

$X = N\sigma_a$ (N is the atom density of the foil per unit area, and σ_a is the cross section at 2200 m/sec.)

$E_3(X)$ = exponential integral

The function is plotted in Figure A-1. The thermal flux depression factors used in the experiments using Type II fuel are summarized in Table A-1.

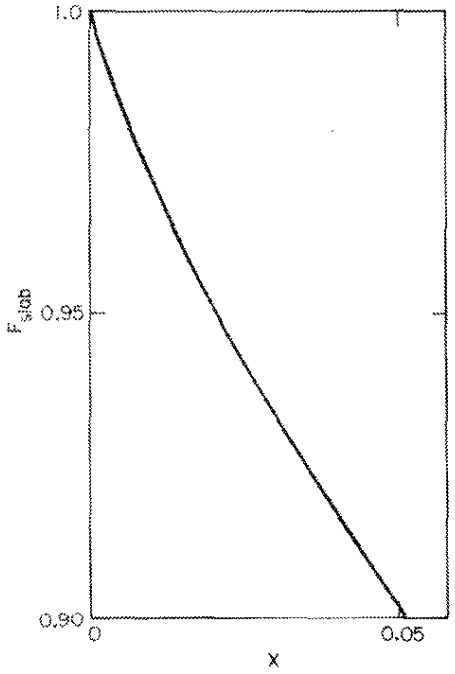

FIGURE A-1. Thermal Isotropic Flux Depression Factors

TABLE A-1

Summary of Thermal Flux Depression Factors for Type II Fuel

Foil							
Gap, cm	*Material*	*Thickness, cm*	X_{Fuel}	X_{Foil}	F_{Fuel}	F_{Foil}	$\frac{F_{Fuel}}{F_{Foil}}$
0.033	Cu	0.0267	0.0162	0.0086	0.959	0.976	0.983
0.015	Depl U	0.0081	0.0075	0.0011	0.979	0.997	0.982
0.028	Paired Nat U and Depl U	0.0191	0.0137	0.0051	0.965	0.985	0.979
0.020	^{235}U-Al	0.0127	0.0098	0.0034	0.973	0.990	0.983

APPENDIX B – FOIL GAP CORRECTION FOR ρ_{28} MEASUREMENT

Factors of 0.99 and 0.98 were used to correct the ^{238}U resonance capture activities in the inner and outer fuel respectively for the increase in resonance capture caused by the 1-mil gap at the detector foils. These factors were derived from a foil gap experiment using Type I fuel in which known gaps ranging from 1 to 21 mils were introduced by aluminum spacers placed on both sides of bare depleted uranium detector foils. The Type I fuel and foil-bearing irradiation assembly are similar to the Type II so that the corrections derived are applicable to the Type II measurements. The experiment was done at a 5.5-inch pitch to accentuate resonance capture effects. The ^{239}Np subcadmium activity component of each foil was derived from previously measured values of ρ_{28} (inner fuel) and ρ_{28} (outer fuel) for the 1-mil gap case after correction for the difference in the thermal flux peaking. Analytically,

$$\left[{}^{239}Np\right]_{\text{Sub-Cd}}^{\text{x-mil gap}} = \frac{\left[{}^{239}Np\right]_{\text{Sub-Cd + Epi-Cd}}^{\text{1-mil gap}}}{\left[1 + \rho_{28}\right]_{\text{Meas}}^{\text{1-mil gap}}} \cdot \frac{\left[\frac{f_{\text{Type I Fuel}}}{f_{\text{Foil}}}\right]_{\text{1-mil gap}}}{\left[\frac{f_{\text{Type I Fuel}}}{f_{\text{Foil}}}\right]_{\text{x-mil gap}}}$$

where

f_{Foil} = thermal flux depression factor of the combined foil and aluminum spacers

$f_{\text{Type I Fuel}}$ = thermal flux depression factor of an equivalent thickness fictitious foil made of Type I fuel

The normalized ^{239}Np epicadmium component of each foil was plotted versus foil gap thickness and extrapolated to zero gap to obtain the correction factors as shown in Figures B-1 and B-2.

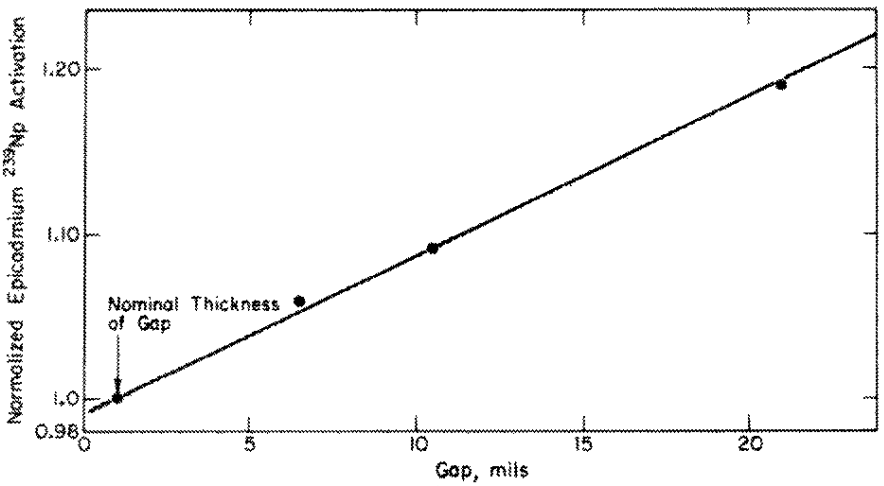

FIGURE B-1. Foil Gap Correction for Inner Type I Fuel

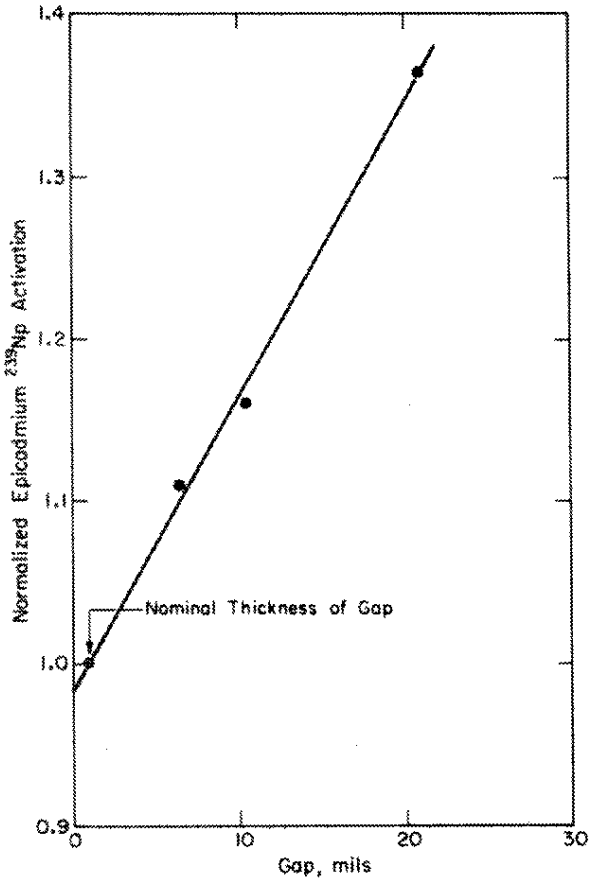

FIGURE B-2. Foil Gap Correction for Outer Type I Fuel

APPENDIX C – FISSION PRODUCT CORRECTION FOR ρ_{28} MEASUREMENT

The fission product activity in the 90-116 keV window for the natural and depleted uranium foils in the fuel was extrapolated to zero by the following correction:

$$A_{Np}^{90-116} = \left(A_{Np} + A_{UFP}\right)_{Meas}^{90-116} - R\left(A_{UFP}^{>500}\right)$$

where

$\left(A_{Np} + A_{UFP}\right)_{Meas}^{90-116}$ = measured activity in the 90-116 keV window [consists of components due to ^{239}Np decay (A_{Np}^{90-116}) and decay of uranium fission products (A_{UFP}^{90-116})]

$R = \dfrac{A_{UFP}^{90-116}}{A_{UFP}^{>500}}$ = ratio of uranium fission product activity in 90-116 keV window (A_{UFP}^{90-116}) to the uranium fission product activity at an integral bias of 500 keV ($A_{UFP}^{>500}$)

In general, R is a function of counter geometry, exposure time after irradiation, and foil thickness. The ratio R was determined for the actual counting conditions and irradiation times of each experiment by including natural and depleted uranium foils in a common flux at the thermal reference position and counting these foils with the natural and depleted uranium foils from the lattice. The activities of natural and depleted uranium foils in a thermal flux are given by

$$A_N^{90-116} = A_{Np}^{90-116} + A_{^{235}UFP}^{90-116} \qquad \text{(C-1)}$$

$$A_D^{90-116} = \left(\frac{N_D}{N_N}\right)^{238}\left(A_{Np}^{90-116}\right) + \left(\frac{N_D}{N_N}\right)^{235}\left(A_{UFP}^{90-116}\right) \qquad \text{(C-2)}$$

$$A_N^{>500} = A_{^{235}UFP}^{>500} \qquad \text{(C-3)}$$

$$A_D^{>500} = \left(\frac{N_D}{N_N}\right)^{235}\left(A_{^{235}UFP}^{>500}\right) \qquad \text{(C-4)}$$

where

A_N^{90-116}, A_D^{90-116}, $A_N^{>500}$, $A_D^{>500}$ represent natural (N) or depleted (D) uranium foil activity per ^{238}U atom in the 90-116 keV window or at the integral bias >500 keV.

$A_{^{235}UFP}^{90-116}$, $A_{^{235}UFP}^{>500}$ represent natural uranium foil fission product activity per ^{238}U atom from ^{235}U fission in the 90-116 keV window or at the integral bias >500 keV.

A_{Np}^{90-116} represents the natural uranium foil ^{239}Np decay activity per ^{238}U atom in the 90-116 keV window.

N_N^{235}, N_D^{235}, N_N^{238}, N_D^{238} represent natural or depleted atom densities for ^{235}U or ^{238}U.

Equations C-2 and C-4 can be rewritten as

$$A_D^{90-116}\left(\frac{N_N}{N_D}\right)^{238} = A_{Np}^{90-116} + \Delta\, A_{^{235}UFP}^{90-116} \qquad \text{(C-5)}$$

and

$$A_D^{>500}\left(\frac{N_N}{N_D}\right)^{238} = \Delta\, A_{^{235}UFP}^{>500} \qquad \text{(C-6)}$$

where

$$\Delta = \left(\frac{N_D}{N_N}\right)^{235}\left(\frac{N_N}{N_D}\right)^{238}$$

Subtracting Equation C-5 from C-1,

$$A_N^{90-116} - A_D^{90-116}\left(\frac{N_N}{N_D}\right)^{238} = A_{^{235}UFP}^{90-116}\,(1 - \Delta) \qquad \text{(C-7)}$$

Subtracting Equation C-6 from C-3,

$$A_N^{>500} - A_D^{>500}\left(\frac{N_N}{N_D}\right)^{238} = A_{^{235}UFP}^{>500}\,(1 - \Delta) \qquad \text{(C-8)}$$

Forming the ratio R' of Equation C-7 to C-8,

$$R' = \frac{A_N^{90-116} - A_D^{90-116}\left(\frac{N_N}{N_D}\right)^{238}}{A_N^{>500} - A_D^{>500}\left(\frac{N_N}{N_D}\right)^{238}} = \frac{A_{235}^{90-116}{}_{UFP}}{A_{235}^{>500}{}_{UFP}} \qquad \text{(C-9)}$$

Making the assumptions that the same ratio applies to ^{238}U fission products (i.e., the fission product distribution for ^{238}U fission is closely identical to that for ^{235}U fission) and that the ^{235}U fission product distribution does not depend strongly on neutron energy, then

$$R = R' = \frac{A_{235}^{90-116}{}_{UFP}}{A_{234}^{>500}{}_{UFP}} = \frac{A_{238}^{90-116}{}_{UFP}}{A_{238}^{>500}{}_{UFP}} = \frac{\left[A_{235}{}_{UFP} + A_{238}{}_{UFP}\right]^{90-116}}{\left[A_{235}{}_{UFP} + A_{238}{}_{UFP}\right]^{500}} \qquad \text{(C-10)}$$

The ratio R is obtained more accurately from the natural and depleted uranium foils in the thermal column irradiation than would be obtained from the natural and depleted uranium foils in the lattice fuel for two reasons:

- In a purely thermal flux (no ^{238}U resonance capture), the desired fission product activity is larger relative to the ^{239}Np activity, which for this determination is an undesired background.
- The ^{239}Np activity in a thermal flux irradiation is quite insensitive to foil geometry imperfections.

APPENDIX D – FOIL THICKNESS CORRECTION FOR ρ_{28} MEASUREMENT

A γ-ray self-attenuation correction must be applied to account for the difference in γ-ray absorption with foil thickness when the natural and depleted uranium foil activities in the ρ_{28} measurement are compared. This correction is particularly important to the uranium foil-counting data in the 90-116 keV window because of the large mass absorption coefficient of uranium in the 90-116 keV region. To estimate the effect of self-attenuation in thin uranium foils, the simple model shown below is used. The distance, d, from the foil to the detector was sufficiently large so that only the path through the foil normal to the surface is considered.

The correction is derived by assuming a uniform distribution of gamma activity in the uranium foil of thickness x_o. The activity of a thin element $dx(A_{dx})$ is given by $A_{dx} \propto dx$. The measured activity contribution of $dx(A_{dx})_M$ at the detector is given by

$$(A_{dx})_M = k\, e^{-\mu x}\, dx$$

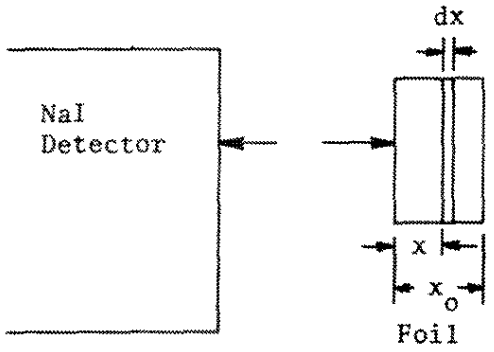

where

k = k (time, exposure, geometry)

μ = linear absorption coefficient for uranium in the 90-116 keV window

The measured activity of the foil (A_M) is then

$$A_M = k \int_o^{x_o} e^{-\mu x}\, dx = \frac{k}{\mu}\,(1 - e^{-\mu x_o})$$

The actual or true activity of the foil without attenuation is given by

$$A_T = kx_o$$

so

$$A_T = \frac{\mu x_o}{1 - e^{-\mu x_o}} A_M$$

μ is determined from a simple transmission experiment for the 90-116 keV energy window by shielding an irradiated ^{238}U foil with different thicknesses of unirradiated ^{238}U absorber.

The linear absorption coefficient is given as the slope of the straight line fit on a semilog plot of the counting rate versus added absorber (Figure D-1). For uranium in the 90-116 keV window, $\mu = -0.0627$ mil^{-1}. The attenuation corrections for the natural and depleted uranium foils in the ρ_{28} measurements are given in Table D-1.

TABLE D-1

Gamma Attenuation Corrections

	Depleted Uranium	*Natural Uranium*
Foil thickness, mils	3.2	4.3
$\frac{\mu x_o}{1 - e^{-\mu x_o}}$	1.107	1.146

The effect of self-attenuation is a small correction (~3.5%) for the difference in thickness between the natural and depleted uranium foils used in the measurements.

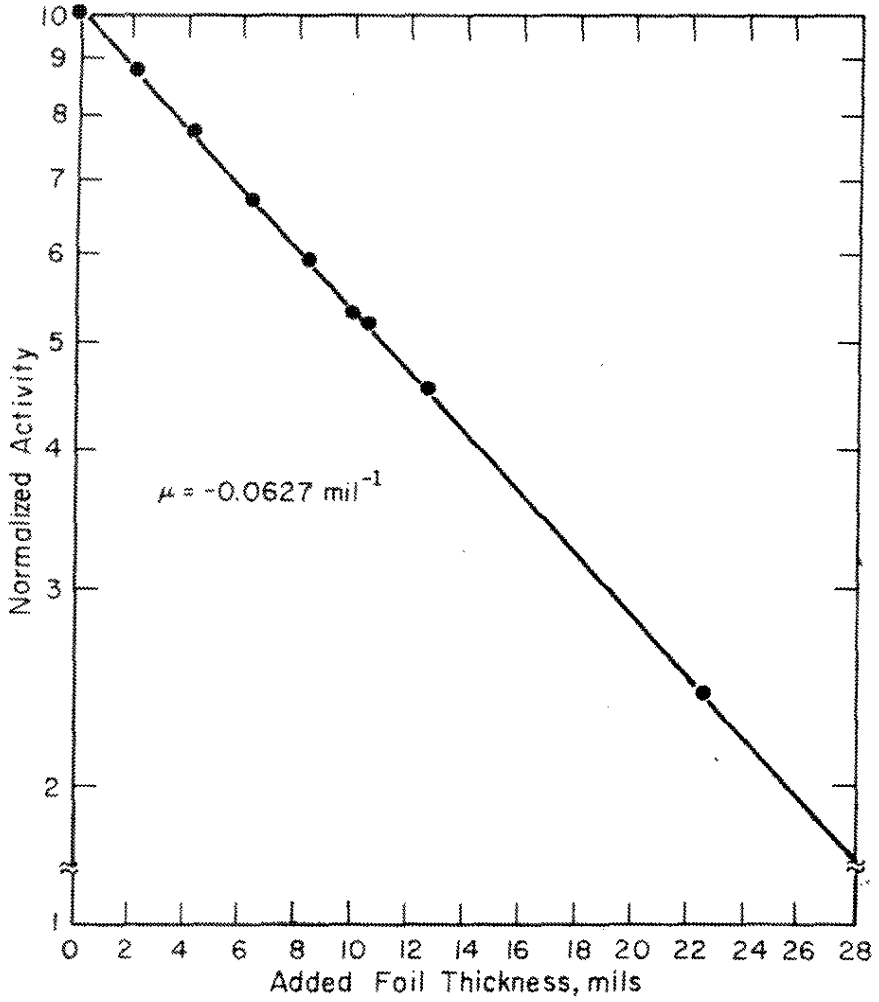

FIGURE D-1. Uranium Metal Gamma Attenuation in 90-116 keV Window

APPENDIX E – AXIAL ELEVATION CORRECTION

Corrected foil activities were reduced to a common axial elevation by correction factors derived from the measured axial flux profile in each experiment. The shape of the axial flux was measured by activation of 15 gold pins (1/4-inch x 1/16-inch diameter) placed at 2-inch intervals on a bead chain that was suspended near the center hex. For the cases where $B_m^2 < B_R^2$, the gold pin activations were fit to a simple exponential decay function over the ~8-inch region where the experimental foils were located, and this function was used for the foil elevation corrections. For the more reactive lattice case where $B_m^2 > B_R^2$, the elevation corrections were obtained directly from a smooth curve fit of the gold pin activations.

APPENDIX F – MEASUREMENT OF $(\delta_{28})^{Nat}_{Ref}$

The value of $(\delta_{28})^{Nat}_{Ref}$ was determined by simultaneous irradiation of foils at the reference position and direct measurement of P(t) using a double-chambered fission counter with thin films of depleted and natural uranium as fissioning elements and with natural and depleted uranium foils contained between the two fission chambers. During irradiation, the relative number of fissions (R) occurring in the two films was determined by counting pulses from both chambers. After irradiation, the relative fission product gamma activities of the foils in the fission chambers and at the reference position were determined by counting with a NaI scintillation spectrometer. Since the foils and the films in the double-chambered fission counter were in the same flux, the same relative number of fissions occurred in the foils as in the films and P(t) is given by

$$P(t) = \left[\frac{\left(\frac{N_D}{N_N}\right)^{235} - F}{F - \left(\frac{N_D}{N_N}\right)^{238}}\right]\left[\frac{\left(\frac{N_D}{N_N}\right)^{238} - \gamma(t)}{\gamma(t) - \left(\frac{N_D}{N_N}\right)^{235}}\right]$$

where

$\gamma(t)$ = ratio of the specific gamma activity of the depleted uranium foils to the specific gamma activity of the natural uranium foils contained in the fission counter

F = ratio of the specific fission rate in the chambers containing the depleted uranium film to the specific fission rate in the chamber containing the natural uranium film

N = atom density of the natural (N_N) or depleted (N_D) uranium foils

With simultaneous irradiation of foils at the reference location and in the fission counter, the value of $(\delta_{28})^{Nat}_{Ref}$ is given by

$$(\delta_{28})^{Nat}_{Ref} = \left[\frac{a - F}{F - b}\right]\left[\frac{b - \gamma(t)}{\gamma(t) - a}\right]\left[\frac{\gamma'(t) - a}{b - \gamma'(t)}\right]$$

where

$\gamma'(t)$ = ratio of the specific gamma activity of the depleted uranium foil to the specific gamma activity of the natural uranium foil at the reference position in the 1-inch diameter uranium rod

$$a = \left(\frac{N_D}{N_N}\right)^{235}$$

$$b = \left(\frac{N_D}{N_N}\right)^{238}$$

Thin natural uranium and depleted uranium films for the fission chamber were prepared by electrospraying approximately 0.008 g onto 5/8-inch-diameter stainless steel backings. After deposition, the films were fixed by baking at 200°C for 1/2 hour in an oven.

The relative masses of the thin uranium films used in the fission counter were determined by an auxiliary fission rate measurement in a pure thermal flux in the SP thermal column. The relative mass ratios were determined from the known isotopic composition of the uranium used in the preparation of the films.

The isotopic composition of the depleted uranium foils for the $\gamma(t)$ measurements was determined by activation of the foils in a fully thermalized neutron flux, thus eliminating fission product activity from fast fission in ^{238}U. Natural uranium foils of the same size and thickness were included in the activation to provide a normalization to a known ^{235}U isotopic abundance. The natural and depleted uranium used in the preparation of the thin films for the fission counter were taken from the same stock material used for the foils.

Four experiments were performed to determine $(\delta_{28})^{Nat}_{Ref}$. The fission counter was located inside a Type I fuel outer slug that was in turn surrounded by seven Type I fuel inner slugs.

This arrangement was designed to improve the depleted uranium counting rates by boosting the fast flux at the fission counter. The entire assemblage was surrounded by graphite to improve the thermal fission rate in the Type I fuel flux boosters and located near the side of the SP reactor. Each of the four experiments was completed with a different combination of depleted and natural uranium films in the fission counter. The fission product gamma activities of the natural and depleted uranium foils in the fission counter and in the 1-inch-diameter reference rod were measured with a bias of 500 keV during the time interval from 4 to 8 hours after irradiation. The experimental results are summarized in Table F-1. An average value of $(\delta_{28})^{Nat}_{Ref} = 0.076 \pm 0.001$ was obtained. No corrections have been made for the small differences in flux depression and gamma attenuation between the 2-mil-thick natural uranium foils and the 3-mil-thick depleted uranium foils.

TABLE F-1

Summary of Fast Fission Measurement Data

	Experiments			
	1	*2*	*3*	*4*
$\gamma(t)$	0.1367	0.1409	0.1432	0.1413
$\gamma'(t)$	0.08622	0.08754	0.08633	0.08610
F	0.1498	0.1509	0.1569	0.1580
$(\delta_{28})^{Nat}_{Ref}$	0.076	0.075	0.076	0.078

The measured value of $(\delta_{28})^{Nat}_{Ref}$ is checked for accuracy by using the reference technique to determine δ_{28} for an isolated 1-inch-diameter natural uranium rod in a thermal neutron flux. The measurement was made with a simultaneous irradiation of 1/2-inch-diameter natural and depleted uranium foils in the $(\delta_{28})^{Nat}_{Ref}$ geometry and 1-inch-diameter natural and depleted uranium foils of the same stock in an isolated 1-inch-diameter by 8-inch-long natural uranium rod. The 1-inch-diameter rod was positioned in the center of a 12 × 13 × 14-inch air cavity surrounded by 4-inch-thick graphite placed adjacent to the SP. The fission product gamma activities were determined by counting with an approximate 1.3-MeV bias during the time interval from 2 to 4 hours after irradiation. A measured value of 0.053 ±0.005 is in good agreement with a careful measurement by Bigham[11] of 0.050 ±0.001.

APPENDIX G – DETERMINATION OF $g_{Th\ Ref}$

An index related to the thermal neutron energy spectrum is obtained experimentally by activation of copper and lutetium foils. The ratio ($g_{Lattice}$) of the subcadmium activities of ^{177}Lu and ^{64}Lu from foils in the lattice cell normalized to the same ratio ($g_{Th\ Ref}$) from foils in a pure Maxwellian spectrum at the thermal reference is used for direct comparison with RAHAB calculations.

This type of experiment can be simulated by calculation. The relative foil activations for ^{63}Cu and ^{176}Lu at each cell geometry subregion are presented in the RAHAB code edit option. The equivalent ratio ($g_{Th\ Ref}$) for a Maxwellian flux (used for the normalization) was calculated from the same multigroup cross sections used in the RAHAB calculations.

The Maxwellian distribution of velocities is given by

$$dn = \frac{4n}{\sqrt{\pi}} \frac{v^2}{v_o^3} e^{-\left(\frac{v}{v_o}\right)^2} dv$$

where dn is the number of neutrons per unit volume in the velocity range dv at the velocity v, and n is the total number of neutrons per unit volume. The velocity v_o is the most probable velocity. The Maxwellian distribution of flux [d(nv)] is given by

$$d\phi = d(nv) = \frac{4n}{\sqrt{\pi}} \left(\frac{v}{v_o}\right)^3 e^{-\left(\frac{v}{v_o}\right)^2} dv$$

or in terms of a dimensionless variable $V = \frac{v}{v_o}$

$$d\phi = \frac{4n}{\sqrt{\pi}} V^3 e^{-V^2}$$

Dividing the thermal region into small energy groups or bands, the flux in group i is

$$\phi_i = \frac{4n}{\sqrt{\pi}} V_i^3 \, e^{-V_i^2} \Delta V_i$$

The reaction rate contribution of group i is

$$A_i = \phi_i \sigma_i$$

where σ_i is the average cross section of the i^{th} group. The total reaction rate or activity is then $\sum \phi_i \sigma_i$.

Table G-1 contains a listing by energy group of the velocity V_i, the group width ΔV_i, the neutron flux ϕ_i, the cross section σ_i (for ^{176}Lu and ^{63}Cu), and the product $\phi_i \sigma_i$. The accuracy of

$$g_{Th\ Ref} = \frac{\left(\sum_i \phi_i \sigma_i\right)_{Lu}}{\left(\sum_i \phi_i \sigma_i\right)_{Cu}} = 694.24$$

was verified in a test problem at a 48-inch pitch using Type II fuel. $R \rightarrow 1.00$ at the cell boundary, and $R = 1.0032$ at 46.9 inches from the center of the cell.

TABLE G-1

Determination of $g_{Th\ Ref}$

Energy Group	V_i	ΔV_i	Φ_i	^{176}Lu σ_i, barns	^{176}Lu Φ_i, σ_i	^{63}Cu σ_i, barns	^{63}Cu Φ_i, σ_i
56	4.7475	0.505	9×10^{-9}	43.0	4×10^{-7}	0.949	—
57	4.2725	0.445	4.1×10^{-7}	74.5	3×10^{-5}	1.093	—
58	3.8550	0.39	7.85×10^{-6}	143.0	1.12×10^{-3}	1.290	1.0×10^{-5}
59	3.4900	0.34	7.417×10^{-5}	298.7	2.215×10^{-2}	1.487	1.10×10^{-4}
60	3.1725	0.295	4.008×10^{-4}	684.0	2.7417×10^{-1}	1.681	6.74×10^{-4}
61	2.8975	0.255	1.4012×10^{-3}	1743.6	2.44307	1.870	2.620×10^{-3}
62	2.6600	0.22	3.5009×10^{-3}	4895.1	17.1370	2.053	7.187×10^{-3}
63	2.4550	0.19	6.7827×10^{-3}	11304.2	76.6733	2.228	1.5112×10^{-2}
64	2.2775	0.165	1.08936×10^{-2}	12265.9	133.6196	2.396	2.6101×10^{-2}
65	2.1225	0.145	1.53254×10^{-2}	8128.4	124.5710	2.559	3.9218×10^{-2}
66	1.980	0.14	2.15534×10^{-2}	5309.9	114.4463	2.719	5.8604×10^{-2}
67	1.845	0.13	2.71383×10^{-2}	3837.1	104.1325	2.888	7.8375×10^{-2}
68	1.720	0.12	3.16920×10^{-2}	3048.5	96.6131	3.058	9.6914×10^{-2}
69	1.605	0.11	3.45991×10^{-2}	2594.5	89.7673	3.230	1.11755×10^{-1}
70	1.50	0.1	3.55722×10^{-2}	2381.2	84.7046	3.401	1.20981×10^{-1}
71	1.40	0.1	3.86516×10^{-2}	2142.1	82.7955	3.579	1.38334×10^{-1}
72	1.30	0.1	4.05389×10^{-2}	2026.9	82.1684	3.773	1.52953×10^{-1}
73	1.20	0.1	4.09411×10^{-2}	1960.0	80.2446	3.988	1.63273×10^{-1}
74	1.10	0.1	3.96901×10^{-2}	1936.6	76.8638	4.228	1.67810×10^{-1}
75	1.00	0.1	3.67879×10^{-2}	1953.8	71.8763	4.541	1.67054×10^{-1}
76	0.90	0.1	3.24302×10^{-2}	2014.0	65.3143	5.196	1.68507×10^{-1}
77	0.80	0.1	2.69974×10^{-2}	2123.3	57.3235	6.035	1.62929×10^{-1}
78	0.70	0.1	2.10131×10^{-2}	2294.8	48.2208	7.066	1.48479×10^{-1}
79	0.60	0.1	1.50698×10^{-2}	2555.9	38.5169	8.370	1.26134×10^{-1}
80	0.50	0.1	9.7351×10^{-3}	2955.3	28.7699	10.087	9.8198×10^{-2}
81	0.40	0.1	5.4537×10^{-3}	3589.4	19.5756	12.476	6.8040×10^{-2}
82	0.30	0.1	2.4676×10^{-3}	4655.5	11.4880	16.098	3.9723×10^{-2}
83	0.20	0.1	7.686×10^{-4}	6863.1	5.2752	22.769	1.7500×10^{-3}
84	0.10	0.1	9.9×10^{-5}	13601.4	1.3466	45.116	4.466×10^{-3}
				$\Sigma =$	1514.185		2.18106

$g_{Th\ Ref} = 694.24$

REFERENCES

1. J. E. Suich and H. C. Honeck. *The HAMMER System - Heterogeneous Analysis by Multigroup Methods of Exponentials and Reactors.* USAEC Report DP-1064, E. I. du Pont de Nemours and Co., Savannah River Laboratory, Aiken, S. C. (1967).

2. H. C. Honeck. *The JOSHUA System.* USAEC Report DP-1380, E. I. du Pont de Nemours and Co., Savannah River Laboratory, Aiken, S. C. (1975).

3. F. J. McCrosson. "Thermal Data Testing of ENDF/B-III and Prognosis for ENDF/B-IV." *Trans. Am. Nucl. Soc. 18,* 352 (1974).

4. J. Hardy, Jr., D. Klein, and J. J. Volpe. "A Study of Physics Parameters in Several H_2O-Moderated Lattices of Slightly Enriched and Natural Uranium." *Nucl. Sci. Eng. 40,* 101 (1970).

5. T. J. Thompson, I. Kaplan, and M. J. Driscoll (editors). *Heavy Water Lattice Project Final Report.* USAEC Report MIT-2344-12, Massachusetts Institute of Technology, Department of Nuclear Engineering, Cambridge, Mass. (1967).

6. A. E. Dunklee and C. E. Jewell. *Zero-Power Measurements on a High-Flux Demonstration Lattice.* USAEC Report DP-1076, E. I. du Pont de Nemours and Co., Savannah River Laboratory, Aiken, S. C. (1967).

7. R. C. Axtmann, L. A. Heinrich, R. C. Robinson, O. A. Towler, and J. W. Wade. *Initial Operation of the Standard Pile.* USAEC Report DP-32, E. I. du Pont de Nemours and Co., Savannah River Laboratory, Aiken, S. C. (1953; Declassified 1957).

8. J. L. Jarriel and D. J. Pellarin. *SRL Experiments for the Japanese Power Reactor and Nuclear Fuel Development Corporation.* USAEC Report DP-1219, E. I. du Pont de Nemours and Co., Savannah River Laboratory, Aiken, S. C. (1970).

9. P. B. Kemshell. *Some Integral Properties of Nuclear Data Deduced from WIMS Analyses of Well Thermalised Uranium Lattices.* Report AEEW-R-786, Atomic Energy Establishment, Winfrith, England (1972).

10. N. P. Baumann. *Resonance Integrals and Self-Shielding Factors for Detector Foils.* USAEC Report DP-817, E. I. du Pont de Nemours and Co., Savannah River Laboratory, Aiken, S. C. (1963).

11. C. B. Bigham. *Measurement of Fast Fission Ratios in Natural Uranium.* Report AECL-2285 (CRRP-1220), Atomic Energy of Canada Ltd., Chalk River, Ontario Canada (1965).